

Optimal sensing of urban road networks with large-scale ridesourcing vehicles

Shuocheng Guo^a, Xinwu Qian^{a,*}

^a*Department of Civil, Construction and Environmental Engineering, The University of Alabama, Tuscaloosa, AL 35487, United States*

Abstract

The monitoring of the urban road network contributes to the efficient operation of the urban transportation system and the functionality of urban systems. Current practices of sensing urban road networks mainly depend on inductive loop sensors, roadside cameras, and crowdsourcing data from massive urban travelers (e.g., Google Map). These data have the drawbacks of high costs, limited coverage, or low reliability due to insufficient user penetration. This study investigates an innovative approach of drive-by sensing, which leverages large-scale ridesourcing vehicles (RVs) to monitor and infer the states of urban road networks. With RV traversing over road networks, we examine the RV fleet sensing performance based on the unique number of road segments explicitly visited, the sensing reliability as a result of repeated visits, and the information that can be implicitly inferred given explicit data and road network topology. We propose an optimal rerouting model to simultaneously maximize the sensing coverage and sensing reliability, which can be efficiently solved using a heuristic algorithm to guide the cruising trajectory of unoccupied RVs sequentially. To validate the effectiveness of the proposed model, comprehensive experiments and sensitivity analyses are performed using real-world RV data of more than 20,000 vehicles in New York City (NYC). Our approach is shown to cover up to 75.5% of all road segments which leads to an implicit coverage of 97.2%. More importantly, the coverage are obtained with at least 31.1% improvements in sensing reliability as compared to the baseline scenario.

Keywords: Mobile crowdsensing, Drive-by sensing, Ridesourcing vehicle, Sensing coverage and reliability

*Corresponding author.

Email addresses: sguo18@crimson.ua.edu (Shuocheng Guo), xinwu.qian@ua.edu (Xinwu Qian)

1. Introduction

The sensing and monitoring of dynamic states in urban road networks (e.g., traffic flow, road congestion, and air quality) are critical to the effective functionality of our cities. As a conventional approach, sensing and monitoring are achieved using fixed-location-location sensors such as inductive loop detectors and roadside cameras. These approaches suffer reliability drawbacks and financial concerns on installation, operation, and maintenance (Yoon et al. 2007, Work et al. 2008). Benefited from the recent advances in portable mobile sensors and cloud computing and the rise of shared mobility services, the combination between drive-by sensing and ridesourcing vehicles (RVs) has shown its potential as a low-cost and reliable alternative for large-scale monitoring the urban environment. In particular, crowdsourcing data can be collected from a fleet of mobile sensor-equipped ridesourcing vehicles (Mora et al. 2019, O’Keeffe et al. 2019), where the vehicle fleet is already on duty 7-24 and traverses across the urban road network to provide mobility services. When equipped with different kinds of mobile sensors, the surveillance through RVs is expected to break the bottlenecks of traditional sensing solutions for a more cost-effective and flexible deployment at scale. The RV sensing can not only assist conventional applications in transportation planning (e.g., real-time travel speed prediction (Cui et al. 2019) and short-term travel demand forecasting (Qian et al. 2020c)) and environmental and infrastructure monitoring (Desouza et al. 2020, Khan et al. 2016). More importantly, it can also uptake emerging sensing tasks such as information broadcasting in the connected vehicle environment Abdelhamid et al. (2014, 2015) and training data collection for autonomous driving Anjomshoaa et al. (2018). A non-comprehensive list of possible applications based on RV sensing is summarized in Table 1 (the categories are adapted from Anjomshoaa et al. (2018)).

Table 1: Potential applications of RV-based driver-by sensing.

Category	Sensor	Application(s)
Ambient Fluid	Air quality monitor	Monitoring air quality
Urban Envelope	Visual camera	Real-time imaging of urban areas and collecting street information
Electromagnetic	GPS and RFID	Monitoring traffic flow and congestion
Electromagnetic	GPS, gyroscope, and accelerometer	Fetching sample trajectories for training autonomous vehicles
Electromagnetic	WiFi and Bluetooth	Constructing vehicle-to-vehicle network

Despite the benefits of RV-based drive-by sensing, there exist three challenges to deliver the

sensing tasks efficiently. First, RV trips are driven by passenger demand and urban mobility needs (Qian et al. 2015). In this regard, high-demand areas may be repetitively visited, resulting in a disproportional sensing coverage and, further, spatial disparity regarding the sensing of urban road network. Second, the mobility service provided by RV fleets is not initially designed for performing sensing tasks. An RV with onboard passengers can hardly deviate from the shorter and faster route to reach a higher sensing coverage. Only the unoccupied RVs can be rerouted for improved sensing performances, but with restricted flexibility due to time constraints (e.g., timely arrival for the next pick-up request). Finally, existing studies showed that complete system information can be inferred based on a partial observation without an explicit visit of the road segment (Ng 2012, He 2013). This suggests a potential direction for enhancing sensing performance if we can understand what additional information can be implicitly inferred based on the explicit visits of road segments by mobile sensor-equipped RVs.

To address the above challenges, this study investigates an optimal sensing strategy for routing RV-based vehicles in monitoring large-scale urban road network. We start by examining the historical sensing performance concerning (1) the proportion of road segments with explicit visits, (2) the sensing reliability considering repeated visits during a period, and (3) the proportion of unvisited road segments whose information can be implicitly inferred from the explicit observations and network topology. To enhance sensing performances, we develop an optimal rerouting model that is formulated as an entropy maximization problem. The model is shown to simultaneously maximize explicit sensing coverage and reinforce sensing reliability. To solve the optimization problem in real-time with high-quality solutions, we further propose a heuristic algorithm that guides unoccupied RVs to the road segment under less sensing frequency sequentially. The effectiveness of our model is comprehensively demonstrated using the real-world RV trajectory data in New York City, covering over 100,000 RVs and more than 1 million daily passenger trips (NYCTLC 2021). Further, sensitivity analyses are conducted regarding the trade-off between the energy consumption and improvement of sensing performance under the optimal rerouting strategy. We note that this study is an extension of our previous work (Guo et al. 2022) that explored the universality of sensing frequency and RV’s driving range, which can be viewed as the baseline for the optimal rerouting strategy investigated in this work. We summarize the major contributions of this study as follows:

- We adopt real-world trip trajectory data to investigate the sensing performance regarding both coverage and reliability under a large-scale RV fleet.
- Based on the knowledge of link observability and road network topology, we develop and validate an optimal rerouting strategy to advise the cruising paths for unoccupied RVs to further improve the sensing performance of both coverage rate and reliability.
- Using a decomposition method, we propose two heuristic algorithms that can provide high-quality rerouting decisions in real-time, which can be easily transferred to real-world scenarios with a sequence of idling RVs to be assigned.
- Comprehensive numerical experiments using real-world trajectory data are conducted to demonstrate the effectiveness of our optimal sensing model and the trade-offs between sensing performances and energy consumption are also investigated.

The rest of the study is organized as follows. In the next section, we briefly review related literature on the transportation sensing problems. In Section 3, we introduce the RV trajectory data and study area. In Section 4, we discuss the methods for measuring the sensing performances using RV trajectory data. And we propose an optimal rerouting strategy to improve the sensing performance, which is solved by one rule-based greedy algorithm and one heuristic algorithm in Section 5. In Section 6, we present a case study on evaluating the RV sensing in the Manhattan area, NYC, and provide a comprehensive discussion on the performances of the vehicle-based drive-by sensing and the trade-off between the additional energy consumption and improvement in the sensing performance. Finally, we summarize the major findings and conclude our study in Section 7.

2. Literature

The sensor placement problem regarding the fixed-location sensors (i.e., inductive loop detectors and roadside cameras) has been extensively investigated in recent decades (for a comprehensive survey, see Gentili and Mirchandani 2018). Among the first, Lam and Lo (1990) proposed two key components to select the optimal sensor locations: traffic flow volume and origin-destination (OD) coverage. Yang et al. (1991) evaluated the performance of the OD flow estimation based on the traffic volume counts. Later, researchers proposed different optimization-based frameworks

to find the optimal sensor placement considering the travel time estimation and traffic OD flow count (Yang and Zhou 1998, Ban et al. 2009, Zhou and List 2010, Li and Ouyang 2011). Besides, the reliability of sensor location on the travel time estimation (Fujito et al. 2006, Ban et al. 2007) and OD coverage (Fei et al. 2007, 2013) has also been investigated. With a limited budget for fixed-location sensors, complete coverage on every road segment can hardly be achieved. In addition to the optimal sensor location design, it motivates the researchers on the link observability problem, where the information (e.g., traffic volumes) can be inferred based on the historical observation and road network topology with no sensors being physically installed (Hu et al. 2009, Ng 2012, Viti et al. 2014, Xu et al. 2016). The advances in the global positioning system (GPS) technology make it feasible and practical to conduct dynamic probing for the traffic condition. In this case, the data are collected from the GPS-enabled mobile devices or smartphones (Work et al. 2008, Herrera et al. 2010), mobile traffic sensors (Sun and Ban 2013), and Bluetooth sensors (Park and Haghani 2015).

Most recently, with the advances in the mobile portable sensors and efficient online cloud-computing platform (Mora et al. 2019), the feasibility of *drive-by sensing* has been initially examined in various cities in the world (O’Keeffe et al. 2019, Anjomshoaa et al. 2020, Ma and Qian 2021, Guo et al. 2022). In particular, the drive-by sensing by the RV fleet has shown great merits in addressing the barriers in the fixed-location sensor regarding the data reliability and coverage issues, which usually requires an extremely large amount of investment to achieve both. One feature of RV-based drive-by sensing is the flexibility, where a slight deviation from the original routes may significantly enhance the coverage of sensing without additional cost on the new fixed-location sensor construction. In addition, the drive-by sensing fleet can provide the data in high spatial and temporal resolution (Anjomshoaa et al. 2020), which can accurately capture dynamic features in the environment (i.e., air pollutants, air pressure, spatial temperature differences (Anjomshoaa et al. 2018)).

So far, few studies have investigated the feasibility and efficiency of large-scale RV-based drive-by sensing in urban areas. There are two studies focusing on the sensing performance of the drive-by sensing using the historical taxi trip data. Specifically, Agarwal et al. (2020) examined the explicit sensing coverage of drive-by sensing in San Francisco and Rome using 1,138 and 304 vehicles, respectively. O’Keeffe et al. (2019) proposed sensing power to statistically quantify the sensing reliability under different fleet sizes using the taxi trip data in nine major cities. However,

both studies stayed at the explicit observations based on historical trips with no redeployment to improve the sensing performance. Distinct from those, our study first explores the potential improvement in sensing coverage by inferring the information on the unvisited road segments. And the optimal rerouting strategy can further enhance the sensing performance of the RV-based drive-by sensing. Both the information inference and the redeployment of the large-scale fleets have not been investigated in the field of RV-based drive-by sensing.

3. Data

We use the RV trajectory data in Manhattan, New York City (NYC), to gain insights into the sensing range of the RV fleet over the urban road network. We collected the RV trajectory data in April 2017 using the method as described in Qian et al. (2020b). The collected trajectory records include the information of timestamp (in Unix), latitude, longitude, and driver ID (only the last six letters shown here). A sample of collected trajectory records can be seen in Table 2.

Table 2: Sample data records

Driver ID	Epoch	Latitude	Longitude
4d9ded	1492341210000	40.595	-73.951
621df1	1492350555000	40.835	-73.863
7505ef	1492373010000	40.599	-73.951
2b8d71	1492334100000	40.661	-73.792
218d52	1492396650000	40.655	-73.882

3.1. Data processing

We fetched around 100 GB of data per day in 2017 by constructing 470 data collection stations. The data quality was validated by inferring the number of actual trips and comparing with the reported trips to the transportation network companies for every 15-minute time interval of the entire city (Qian et al. 2020a). Specifically, one complete trip is identified if (1) the time gap ($\Delta t \geq 10\text{min}$) and spatial displacement ($\Delta d \geq 1\text{km}$) between consecutive records or (2) the record was the last trajectory identified for the driver ID. In addition, we consider the trip with a time gap $\Delta t \geq 120\text{min}$ as an online/offline transition. In this case, we split the trajectories into two shifts and conduct the trajectory processing within the shifts.

After identifying occupied trips from the trajectory of vacant vehicles, we next augment the initial set of vacant trajectories with the inferred trajectories of the occupied trips. For the trajec-

ries of the vacant trips, we only adopt the coordinates per 15-second interval. As for the occupied trips, only the trip’s origin-destination (OD) information is derived, and the detailed trajectory cannot be immediately observed for at least 10 minutes due to the data limitation. In light of this, we next infer the occupied trip trajectory using the trip’s OD information by querying the shortest path in the road network via the Open Source Routing Machine (OSRM) (Luxen and Vetter 2011). The query results from the OSRM consist of the coordinates of traversed intersections and the associated timestamps. Based on that, we further interpolate the sequence of coordinates into 15-second intervals for the sake of consistency.

Having obtained the occupied and vacant trip trajectories, we next match the coordinates to the nearest road segments in the *backbone* network in Manhattan in NYC. In this case, we use sequences of road IDs to represent the trajectories of each RV. Note that the backbone road network only includes ‘primary’ and ‘secondary’ roads according to Boeing (2017), OpenStreetMap contributors (2017), which are specified as below:

- **Primary roads:** Interstate Business Routes, US Routes, US Business routes, and State Routes in dense urban areas.
- **Secondary roads:** State Routes, State Business routes, and major urban streets (streets in urban areas with high amount of traffic).

These backbone roads primarily cover the urban area and are of priority to be sensed. Moreover, regarding our optimal rerouting strategy (see Section 4), the backbone road network can (1) reduce the computational burden under a smaller problem size and (2) diversify the choices of cruising routes using shortest path algorithms (i.e., K -shortest path algorithm (Yen 1971)).

4. Method

This section introduces the metrics to evaluate the sensing performance regarding the coverage and reliability. To improve both of them, we develop an optimal rerouting strategy, which is first solved by a K -shortest path-based heuristic algorithm using a decomposition method. We also propose a rule-based greedy algorithm as a benchmark. Finally, we measure the energy consumption and emissions for the entire RV fleet following optimal rerouting strategy to better understand the

trade-off between energy consumption, emissions, and the improvement of sensing performance.

We summarize the notations in Table 3.

Table 3: Notation

Notation	Description
<u>Sets</u>	
\mathcal{G}	A transportation network, $\mathcal{G} := (\mathcal{N}, \mathcal{A})$
\mathcal{N}	Set of nodes in \mathcal{G}
\mathcal{A}	Set of links in \mathcal{G} , $\mathcal{A} := \mathcal{A}_{ob} \cup \mathcal{A}_{inf} \cup \mathcal{A}_{uob}$
\mathcal{A}_{ob}	Set of observed links
\mathcal{A}_{inf}	Set of inferred links
\mathcal{A}_{uob}	Set of unobserved links
\mathcal{A}_{add}	Set of additional links to be observed to achieve a 100% coverage rate
$\mathcal{A}^-(i)$	Set of links flowing in node $i \in \mathcal{N}$
$\mathcal{A}^+(i)$	Set of links flowing out from node $i \in \mathcal{N}$
$\mathcal{A}(i)$	Subset of link with the corresponding flow information included node $i \in \mathcal{N}$, $\mathcal{A}(i) = \mathcal{A}^-(i) \cup \mathcal{A}^+(i)$
\mathbf{V}	Set of link flows
\mathbf{V}_{ob}	Set of link flows associated with observed links
\mathbf{V}_{inf}	Set of link flows associated with inferred links
\mathbf{V}_{uob}	Set of link flows associated with unobserved links
\mathcal{T}	Set of time slots for the sampled horizon
\mathcal{M}^t	Set of historical cruising trips at $t \in \mathcal{T}$
\mathcal{A}^t	Set of the traversed links by historical cruising trips at $t \in \mathcal{T}$
\mathcal{O}^t	Set of origin nodes at $t \in \mathcal{T}$, $\mathcal{O}^t := \{o_m : m \in \mathcal{M}^t\}$
\mathcal{D}^t	Set of destination nodes at $t \in \mathcal{T}$, $\mathcal{D}^t := \{d_m : m \in \mathcal{M}^t\}$
\mathcal{R}_m	Set of feasible paths for trip $m \in \mathcal{M}^t$ from node $o_m \in \mathcal{O}^t$ to node $d_m \in \mathcal{D}^t$
\mathcal{K}^t	Set of sampled RV fleet size during time period $t \in \mathcal{T}$
$\mathcal{M}^{t,*}$	Set of cruising trips following the optimal rerouting strategy
$\mathcal{A}^{t,*}$	Set of traversed links following the optimal rerouting strategy
<u>Parameter</u>	
t_{ij}	Travel time on link $(i, j) \in \mathcal{A}$
<u>Matrices</u>	
A	Node-link incidence matrix with the dimension of $ \mathcal{N} $ by $ \mathcal{A} $
A_1	An invertible submatrix derived from A with the dimension of $ \mathcal{A} $ by $ \mathcal{A} $
A_2	A complementary matrix derived from A with the dimension of $ \mathcal{A} $ by $ \mathcal{N} - \mathcal{A} $
A_{ob}	An invertible submatrix derived from A where the corresponding links are observed.
A_{uob}	A complementary matrix derived from A where the corresponding links are not explicitly observed.
<u>Variables</u>	
S^t	Sensing power at $t \in \mathcal{T}$
P_{ij}^t	Probability of link $(i, j) \in \mathcal{A}$ being traversed at $t \in \mathcal{T}$
H^t	Entropy of sensing frequency considering all links $i \in \mathcal{A}$ at $t \in \mathcal{T}$
x_{ij}^m	A binary decision variable such that $x_{ij}^m = 1$ indicates that the link $(i, j) \in \mathcal{A}$ is covered by an alternative trip of the sampled trip $m \in \mathcal{M}^t$, and 0 otherwise.
<u>Evaluation Metrics</u>	
c^{exp}	Explicit coverage rate (ECR)
c^{inf}	Inferred coverage rate (InfCR)
c^{imp}	Implicit coverage rate (ImpCR)
C_{mo}	Fuel consumption for moving activities of the RV trajectory.
C_{st}	Fuel consumption for stationary activities of the RV trajectory.
E_{mo}^i	Emission factor i for moving activities of the RV trajectory.
E_{st}^i	Emission factor i for stationary activities of the RV trajectory.

4.1. Link observability

The link observability measures the coverage of RV visits on each road segments at the entire network level. We consider a road network $G = (\mathcal{N}, \mathcal{A})$, where \mathcal{N} is the set of nodes (intersections) and \mathcal{A} is the set of links (road segments). The most straightforward measure of link observability is to consider the explicit observations on road segments collected from the RVs, termed as explicit coverage rate (ECR, c^{exp}), which can be expressed as:

$$c^{exp} = \frac{|\mathcal{A}_{ob}|}{|\mathcal{A}|} \quad (1)$$

where \mathcal{A}_{ob} represents the set of observed (visited) links and $|\mathcal{A}|$ gives the total number of road segments.

In addition to ECR, we note that the certain information (i.e., traffic counts and travel speed) on unobserved (unvisited) links (\mathcal{A}_{uob}) is likely be inferred from the data collected from neighboring links depending on the structure of the road network. Consider a transportation corridor consisting of $2N$ road segments. It can be fully observed by only deploying N fixed sensors on every other road segment. This implies that we can further refine our understanding of the link observability by (1) accounting for the possible number of inferable links (\mathcal{A}_{inf}) based on existing observations on links (\mathcal{A}_{ob}), and (2) identifying the minimum number of additional links (\mathcal{A}) that need to be visited so that the maximal network observability can be achieved. These two new sensing level measures can be formally expressed as the inferred coverage rate (InfCR, c^{inf}) and implicit coverage rate (ImpCR, c^{imp}) as follows:

$$c^{inf} = \frac{|\mathcal{A}_{ob}| + |\mathcal{A}_{inf}|}{|\mathcal{A}|} \quad (2)$$

$$c^{imp} = \frac{|\mathcal{A}_{ob}|}{|\mathcal{A}_{ob}| + |\mathcal{A}_{add}|} \quad (3)$$

The remaining issue is on the identification of \mathcal{A}_{add} . We formulate the link coverage of the RV fleet as a link observability problem under a mobile sensing network. Specifically, we adopt a node-based approach instead of path enumeration (see Hu et al. (2009)), thereby simplifying the problem in a large-scale network (Ng 2012). Given the road network \mathcal{G} , we formally express the node-link incidence matrix as A while only considering nodes in the intersections (Ahuja et al.

1988), which takes the form:

$$A = \begin{bmatrix} a_{11} & a_{12} & \dots \\ \vdots & \ddots & \\ a_{|\mathcal{N}|1} & & a_{|\mathcal{N}||\mathcal{N}|} \end{bmatrix}$$

And for each element a_{ij} in A :

$$a_{ij} = \begin{cases} 1 & j \in \mathcal{A}^+(i) \\ -1 & j \in \mathcal{A}^-(i) \end{cases} \quad (4)$$

where $\mathcal{A}^+(i)$ and $\mathcal{A}^-(i)$ are the set of links associated with node i regarding the outgoing flow and incoming flow, respectively. For every intermediate node in a transportation network, it must be satisfied the flow conservation constraint, which enforces that the total amount of incoming flow is equivalent to the total amount of outgoing flow. We next express the flow conservation condition at node $i \in \mathcal{N}$ as below:

$$A\mathbf{V} = 0 \quad (5)$$

where \mathbf{V} denotes the vector of link flows. Here the incidence matrix A is of dimension $|\mathcal{N}|$ by $|\mathcal{A}|$. Without loss of generality, we assume $|\mathcal{N}| < |\mathcal{A}|$, which is common in a real-world transportation network. We next partition the incidence matrix A into two submatrixs, A_{ob} and A_{uob} , depending on whether the corresponding links are observed or not, and the form follows by $A = \begin{pmatrix} A_{uob} & A_{ob} \end{pmatrix}$. Note that A_{uob} is an $|\mathcal{N}| \times |\mathcal{N}|$ invertible matrix, and the existence of A_{uob} has been proved in Ng's work (see the Proposition 1 in Ng (2012)). And A_{ob} denotes the complementary matrix to A_{uob} . We can therefore rewrite the Equation (5) as below:

$$\begin{pmatrix} A_{uob} & A_{ob} \end{pmatrix} \begin{pmatrix} \mathbf{V}_{uob} \\ \mathbf{V}_{ob} \end{pmatrix} = 0 \quad (6)$$

where the links $i \in \mathbf{V}_{ob}$ indicate the existing observed links and links $j \in \mathbf{V}_{uob}$ denote the remaining unobserved links. We note that the inferred links serve as a subset of unobserved links: $\mathcal{A}_{inf} \subset \mathcal{A}_{uob}$, where the number of inferred links depends on the underlying node-link dependency in submatrix A_{uob} . Based on A_{uob} , we can identify \mathcal{A}_{uob} based on the following steps:

1. Find the reduced row echelon form (RREF) of A_{uob} .

2. If $\text{RREF}(A_{uob})$ is not a full rank matrix, then calculate the RREF of the transpose of $\text{RREF}(A_{uob})$. Eliminate the dependent columns of $\text{RREF}(\text{RREF}(A_{uob})^T)$ to get a new A_{uob} .
3. Set \mathcal{A} as the set of road segments that correspond to the pivot columns of $\text{RREF}(A_{uob})$

Interested readers can refer to Ng (2012) for a more detailed implementation procedure of finding the inferable links based on existing observations.

4.2. Fleet sensing power

Aside from the link observability, we also quantify the sensing reliability by introducing the concept of *sensing power* (O’Keeffe et al. 2019). The sensing power can help to examine if the EV fleet can reproduce the similar sensing pattern during different time periods given the randomness of the drivers’ behavior and the distribution of travel demand. We note that the consistency of sensing performance from the obtained data is of great importance for the decision-making in the large-scale urban network.

Formally, the sensing power denotes the expectation on the probability that one road segment $i \in \mathcal{A}$ can be traversed at least once by the RV fleet during the time period $t \in \mathcal{T}$. By considering the varying coverage rate on different time periods (O’Keeffe et al. 2019), the traversed road segments are more likely to be a strict subset of all road segments ($\mathcal{A}^t \subsetneq \mathcal{A}$), meaning that there exists a non-empty unvisited set of links $\mathcal{A} \setminus \mathcal{A}^t$ for every time period t . In this regard, we aim to examine the *sensing reliability on the traversed links* by randomly sampling RVs and the associated trips from the historical data. In particular, we can statistically understand the trade-off between the RV fleet size and sensing reliability. We express the sensing power as below:

$$S^t \approx 1 - \frac{1}{|\mathcal{A}^t|} \sum_{(i,j) \in \mathcal{A}^t} (1 - P_{ij}^t)^{|\mathcal{R}^t|} \quad (7)$$

where S^t is the sensing power by RV fleet \mathcal{K}^t during time period $t \in \mathcal{T}$. \mathcal{A}^t is the set of traversed road segment during time period $t \in \mathcal{T}$. P_{ij}^t is the sensing frequency of segment $(i, j) \in \mathcal{A}^t$, and the power term $|\mathcal{R}^t|$ denotes the total number of sampled road segments traversed by the fleet \mathcal{K}^t . Finally, the term $(1 - P_{ij}^t)^{|\mathcal{R}^t|}$ represents the probability of road segment $i \in \mathcal{A}$ not being visited by the RV fleet \mathcal{K}^t in the sampled trajectory record during period t .

4.3. Optimal rerouting strategy

In the current RV market, the trip and relocation decisions are largely made based on drivers' own knowledge or following the recommendations from a central dispatch system. However, such a decision making process barely takes the vehicle sensing power perspective into consideration, and there is a significant potential to improve the sensing coverage of RVs without sacrificing their level of service. In this section, we explore the optimal rerouting strategy for RVs by altering the cruising paths in the historical data. While it is restrictive to change the routes of occupied trips due to the data limitation, we only consider alternative routes for the cruising trips in order to maximize the sensing coverage as well as the corresponding reliability.

We consider optimizing the sensing frequency during the time intervals of equal length, denoted by $t \in \mathcal{T}$. Let \mathcal{M}^t denote a set of cruising trips at time interval t . Each element $m \in \mathcal{M}^t$ is represented by a tuple of four elements: $m := (o_m, d_m, T_m^o, T_m^d)$, where o_m and d_m are the origin and destination locations, and T_m^o and T_m^d represent the departure and arrival time at locations o_m and d_m in the historical data, respectively.

Formally, we formulate the optimal rerouting strategy as a entropy maximization problem with respect to the entropy of sensing frequency (H^t) for each time interval $t \in \mathcal{T}$. A small entropy value reflects the skewed distribution of vehicle visiting frequency on each link, while a large entropy value indicates that the visiting counts are more evenly distributed. As such, the corresponding rerouting strategy is expected to simultaneously maximize the sensing coverage and sensing reliability by selecting an alternative path with more unvisited links or/and the links with low sensing frequency (detailed in Appendix Proposition 1).

The optimal rerouting strategy can be expressed as below:

$$\max_x H^t \tag{8}$$

$$\text{subject to } H^t = - \sum_{i \in \mathcal{A}} P_{ij}^t \log P_{ij}^t \tag{9}$$

$$P_{ij}^t = \frac{\sum_{m \in \mathcal{M}^t} x_{ij}^m}{\sum_{m \in \mathcal{M}^t} \sum_{(i,j) \in \mathcal{A}} x_{ij}^m} \quad \forall (i,j) \in \mathcal{A} \tag{10}$$

$$\sum_{j \in \mathcal{N}, j \neq o_m} x_{o_m, j}^m = 1 \quad \forall m \in \mathcal{M}^t \tag{11}$$

$$\sum_{i \in \mathcal{N}, i \neq d_m} x_{i, d_m}^m = 1 \quad \forall m \in \mathcal{M}^t \tag{12}$$

$$\sum_{j \in \mathcal{N} \setminus \{d_m\}} x_{ji}^m - \sum_{j \in \mathcal{N} \setminus \{o_m\}} x_{ij}^m = 0 \quad \forall i \in \mathcal{N}, m \in \mathcal{M}^t \tag{13}$$

$$\sum_{(i,j) \in \mathcal{A}} t_{ij} x_{ij}^m \leq \delta (T_m^d - T_m^o) \quad \forall m \in \mathcal{M}^t \tag{14}$$

$$x_{ij}^m \in \{0, 1\} \quad \forall (i,j) \in \mathcal{A}, m \in \mathcal{M}^t \tag{15}$$

where Constraints (10) define the sensing frequency under the rerouting strategy, and the binary variable $x_{ij}^m = 1$ indicates that link $(i, j) \in \mathcal{A}$ is traversed by the alternated trip of the historical trip $m \in \mathcal{M}^t$. Constraints (11) and (12) enforce that for each trip $m \in \mathcal{M}^t$, the origin and destination locations are traversed exactly once. Constraints (13) are the flow conservation constraints, which ensures the inflows and outflows of the intermediate nodes of trip m are equal. Constraints (14) ensures that the total travel time on the alternative trip cannot exceed the time threshold defined by the historical trip duration and a parameter δ , where $\delta = 1$ indicates the historical scenario.

We note that the problem defined by Eq. (9) is equivalent to maximize the sensing power in Eq. (7) under the same set of constraints. To see this, we first show that the two objective functions are both concave under the same feasible region given identical sets of constraints since we consider the same set of RV fleet in the same road network. Therefore, we only need to show that the solution to the first order condition of the objective function in equation (7) also holds for the first order condition in maximizing the sensing power, which is detailed in Proposition 1.

Proposition 1. *Suppose \mathbf{R}^* is the optimal solution to the maximization of H^t in Eq. (9)), then*

\mathbf{R}^* is also the optimal solution to the maximization of the sensing power in Eq. (7).

Proof. See Appendix A.

The proof of Proposition 1 can be found in the Appendix. We note that the maximum entropy problem is difficult to solve since it is a generalization of vehicle-routing problem, and we propose to solve the maximum entropy problem using a decomposition method by sequentially handling each historical trip $m \in \mathcal{M}^t$ (see details in Section 5). However, such a decomposition method relies on a strong assumption that the optimal rerouting trips $r^* \in \mathcal{R}^{t,*}$ are both time- and spatial-independent. It indicates that one link $(i, j) \in \mathcal{A}$ cannot be traversed more than once within a period of time t in the rerouting strategy. In this regard, we propose an *independence score* (I^t) to validate the assumption using the obtained optimal trips. The independence score is developed based on the cosine distance between the resulted link flow (\mathbf{v}^t) and the expected link flow $\bar{\mathbf{v}}^t$, which can be expressed as below:

$$\mathbf{v}^t = (v_{ij}^t : (i, j) \in \mathcal{A}^{t,*}) = \left(\sum_{m \in \mathcal{M}^t} x_{ij}^m : (i, j) \in \mathcal{A}^{t,*} \right) \quad (16)$$

$$\bar{\mathbf{v}}^t = \mathbf{1}_{|\mathcal{A}^{t,*}|} = (1, 1, \dots, 1) \in \mathbb{R}^{|\mathcal{A}^{t,*}|} \quad (17)$$

where each element v_{ij}^t represents the link-flow on (i, j) during time period t , calculated as the flow aggregation of x_{ij}^m over all possible trips m . $\mathcal{A}^{t,*}$ is the traversed links in the optimal rerouting strategy. The expected link flow is considered as a all-ones vector with the length of $|\mathcal{A}^{t,*}|$, indicating the case that all visited links are exactly traversed once.

Therefore, the independence score can be expressed as:

$$I^t = \frac{\mathbf{v}^t \cdot \bar{\mathbf{v}}^t}{\|\mathbf{v}^t\|_2 \|\bar{\mathbf{v}}^t\|_2} \quad (18)$$

where independence score $I^t = 1$ indicates that the two vectors are perfectly same. It implies that the trips in optimal rerouting strategy are independent and each link $(i, j) \in \mathcal{A}^{t,*}$ is traversed exactly once. And $I^t = 0$ represents two totally different vectors (e.g., all links are visited at least twice in our case).

4.4. Fuel consumption and emission

Besides improving sensing performances, we are also interested in the possible side effects such as additional energy consumption and emissions due to rerouting vehicles. We adopt the COPERT model (Ntziachristos et al. 2009) to provide an empirical estimation. Specifically, we first incorporate the full trajectory into a sequence of road segments and calculate the average speed per segment, denoted by v_{ij} . Next, we further partition the road segments based on the average speed v_{ij} . The road segments with $v_{ij} \geq 5$ km/h are identified as *moving activities*, and the remaining segments are defined as *stationary activities*. The separation of moving and stationary activities can differentiate the statuses of vehicle engine, e.g., idling or in motion, which helps to better measure the consumption and emission in high resolution. Let Δt (s) be the unit idle duration, Δl (km) be the length of the full trajectory, and v (km/h) be the average speed for the moving activities on the trajectory. The calculation of fuel consumption and emission factors (i.e., Carbon Monoxide (CO), Nitrogen Oxides (NO_x), and Hydrocarbon (HC)) are expressed as Eqs. (19)-(22), where the subscripts ‘‘MA’’ and ‘‘SA’’ represent the moving and stationary activities, respectively. We refer the interested readers to Qian et al. (2020b) for more detailed calculation and parameter selection for measuring the energy consumption and emission.

- Fuel consumption, C_{mo} and C_{st} (g):

$$C_{MA} = \frac{217 + 0.253v + 0.00965v^2}{1 + 0.096v - 0.000421v^2} \cdot \Delta l \quad (19)$$

$$C_{SA} = 0.27 \text{ g/s} \cdot \Delta t \quad (20)$$

- Emission factor, E_{mo} and E_{st} (g):

$$E_{MA}^i = (1 - \gamma) \frac{\alpha_{1,i}v^2 + \alpha_{2,i}v + \alpha_{3,i} + \frac{\alpha_{4,i}}{v}}{\alpha_{5,i}v^2 + \alpha_{6,i}v + \alpha_{7,i}} \cdot \Delta l \quad (21)$$

$$E_{SA}^i = \beta_i \Delta t \quad (22)$$

where γ denotes the reduction factor, and the emission parameters $\alpha_{1,i}, \dots, \alpha_{7,i}$ are shown as below:

Table 4: Emission parameter for the RV

Emissions i	$\alpha_{1,i}$	$\alpha_{2,i}$	$\alpha_{3,i}$	$\alpha_{4,i}$	$\alpha_{5,i}$	$\alpha_{6,i}$	$\alpha_{7,i}$	β_i (mg/s)
CO	0	11.4	71.7	0	-0.248	35.4	1	13.889
NO _x	6.53e-6	-1.49e-3	9.29e-2	0	3.97e-5	-1.22e-2	1	0.556
HC	1.2e-5	-1.1e-3	5.57e-2	0	-1.88e-4	3.65e-2	1	2.222

5. Solution algorithms

5.1. K -shortest path-based algorithm

The optimal rerouting strategy can be obtained by solving the constrained entropy maximization problem in Eq. (9). However, we note that the constraints of the entropy maximization problem follow similar format of the vehicle routing problem with time windows, which is NP-hard in the strong sense (Solomon 1987). This implies that the exact solution can be hardly obtained efficiently even for moderate sized instances, whereas our problem concerns road networks with thousands of links and tens of thousands of vehicles. As such, we seek for a heuristic approach to provide an approximated solution in the real time.

To establish a heuristic solution, we can formulate the entropy maximization problem using a decomposition method by assuming that the optimal trips are independent. The assumption of independence roots in the fact that the rerouting solution for trip $m \in \mathcal{M}^t$ in the real-world system may only preserve very weak dependencies. On the one hand, only few drivers would require a simultaneous route decision at fine time scale (e.g., every few seconds) and this decision needs to be carried out in real-time, which makes it difficult to account for routing needs of future cruising trips. This implies that the rerouting problem over the entire time period t can be decomposed into independent subproblems with shorter time windows. On the other hand, for each time window, the origin and destination of each cruising trip may be distinctive in a large-scale road network, suggesting that the resulting path may also be spatially independent and can also be solved separately. In light of these considerations, we decompose the original problem into a sequence of routing decision for each cruising trip, where each cruising trip aims at myopically maximizing the current entropy value (based on the decisions made by previous trips) while preserving the feasibility. This can be achieved by rearranging all trips $m \in \mathcal{M}^t$ within time interval $t \in \mathcal{T}$ in the ascending order of T_m^o . And the route feasibility can be ensured by adopting the K -shortest path algorithm (Yen 1971) with a predefined K until the travel time threshold is violated. We

note that a feasible solution always exist under this approach, which corresponds to the original cruising trajectories as in the historical data. The detailed solution procedure is summarized in Algorithm 1.

Algorithm 1 K-SPH: K-shortest Path-based Heuristic Algorithm

- 1: **Inputs:**
 Sets of trips $m \in \mathcal{M}^t$, $t \in \mathcal{T}$ with the information (o_m, d_m, T_m^o, T_m^d)
 Directed road network $G = (\mathcal{N}, \mathcal{A})$
 - 2: **Outputs:**
 Optimal alternated routes $\mathcal{M}^{t,*}$, P_{ij}^t , H_m^t .
 - 3: **Sort** the set of trip $m \in \mathcal{M}^t$ by the departure time T_m^o
 - 4: **for** $m \in \mathcal{M}^t$ **do**
 - 5: **Conduct** the K -shortest path algorithm and obtain a set of K feasible routes for the original trip m , denoted by $\mathcal{R}_m := \{r_m^k : k = \{1, \dots, K\}\}$.
 - 6: **for** $r_m^k \in \mathcal{R}_m$ **do**
 - 7: **if** $\sum_{(i,j) \in r_m^k} t_{ij} \leq \delta (T_m^d - T_m^o)$ **then** *{*/The generated shortest path satisfies time window constraints in Eq.(14) */}*
 - 8: **Update** P_{ij}^t with $x_{ij}^m = 1, \forall (i, j) \in r_m^*$, following Eq. (10)
 - 9: *{*/Following the historical trip m */}*
 - 10: **Update** P_{ij}^t with $x_{ij}^m = 1, \forall (i, j) \in m$, following Eq. (10)
 - 11: **end if**
 - 12: **Update** H_m^t following Eq. (9).
 - 13: **end for**
 - 14: **Record** $r_m^* \leftarrow \arg \max_{r_m} H_m^t$
 - 15: **end for**
 - 16: **Return** Sets of optimal trips $\mathcal{M}^{t,*} \leftarrow \{r_m^* | m \in \mathcal{M}^t\}$
-

In Algorithm 1, the K-shortest path algorithm (see line 5) is performed for each historical trip $m \in \mathcal{M}^t$, yielding a time complexity of $O(|\mathcal{M}^t|K|\mathcal{N}|^3)$, where the K-shortest path algorithm is $O(K|\mathcal{N}|^3)$ (Yen 1971). The performances of Algorithm 1 depends on parameters K and δ , which affect the quality of the solution quality and the time complexity. In particular, δ denotes the level of relaxation in the time window. It allows additional travel time compared to the historical cruising trip, implying more alternative relocation routes hence a better sensing performance. Given a fixed δ , the choice of K determines the number of candidate relocation routes. If K is a sufficiently large number (e.g., $K \rightarrow \infty$), the resulting solution is optimal as it is equivalent to enumerating all possible rerouting trips. However, this will result in a linearly-increased computational time, which can be costly for large-scale experiments considering the growth factor of $|\mathcal{N}^3|$. In this case, the optimal solution may not be obtained within acceptable computation efforts, and one may prefer

to get a high-quality solution with a low computational cost. This trade-off is further examined in our numerical experiments.

5.2. Rule-based greedy algorithm

We next propose a rule-based rerouting algorithm. Instead of using a K-shortest path algorithm in a nested loop (lines 5-10 in Algorithm 1), we aim at identifying the route with the lowest sensing frequency using the Dijkstra's Algorithm ($O(|\mathcal{A}| \log |\mathcal{N}|)$). In this regard, the RVs are sequentially assigned to the route that are rarely visited while satisfying the time window constraints in Eq. (14). Further, we set a limit on number of links such that no significant detour is permissible.

Algorithm 2 RG: Rule-based Greedy Algorithm

- 1: **Inputs:**
 Sets of trips $m \in \mathcal{M}^t$, $t \in \mathcal{T}$ with the information (o_m, d_m, T_m^o, T_m^d)
 Directed road network $G = (\mathcal{N}, \mathcal{A})$
 - 2: **Outputs:**
 Optimal alternated routes $\mathcal{M}^{t,*}$, P_{ij}^t , H_m^t .
 - 3: **Initiate** sensing frequency $P_{ij}^t \leftarrow 0, \forall (i, j) \in \mathcal{A}$.
 - 4: **Sort** the set of trip $m \in \mathcal{M}^t$ by the departure time T_m^o
 - 5: **for** $m \in \mathcal{M}^t$ **do**
 - 6: **Compute** the shortest path r_m^* using the Dijkstra's Algorithm with the weight on link (i, j) being P_{ij}^t .
 - 7: **if** $\sum_{(i,j) \in r_m^*} t_{ij} \leq \delta (T_m^d - T_m^o)$ **then** *{*/The generated shortest path satisfies time window constraints in Eq.(14) */}*
 - 8: **Update** P_{ij}^t with $x_{ij}^m = 1, \forall (i, j) \in r_m^*$, following Eq. (10)
 - 9: **else** *{*/Following the historical trip m */}*
 - 10: **Update** P_{ij}^t with $x_{ij}^m = 1, \forall (i, j) \in m$, following Eq. (10)
 - 11: **end if**
 - 12: **Update** H_m^t following Eq. (9).
 - 13: **end for**
 - 14: **Return** Optimal alternated routes $\mathcal{M}^{t,*} \leftarrow \{\mathbf{r}_m^* | m \in \mathcal{M}^t\}$
-

6. Results

This section presents the results of our numerical experiments. To better understand the time-varying sensing performance, we divide the RV trip trajectory into six three-hour time intervals based on the trip starting time from 9 AM to 3 AM (the next day). Note that the trajectory information from 3 - 9 AM is unavailable due to the data limitation. For the results, we first focus on the spatial distribution of sensing frequency, the potentiality of information inference, and

sensing reliability using the historical RV trajectory data. Next, we highlight the improvement of sensing performance following the optimal rerouting strategy and discuss the trade-off between sensing performance and energy consumption due to rerouting.

6.1. Historical sensing frequency

We first present the spatial distribution of sensing frequency in Manhattan for three selected time periods on a Wednesday (April 19, 2017). Recall that the sensing frequency is the total number of visits to a specific link traversed by a RV’s trip within a time period (e.g., 3 hours in our case). In addition, we define two terms regarding the connectivity of road segments in the road network, namely *main roads* and *branch roads*. The former indicates more connectivity with a great potential for information inferring. And the latter denotes the secondary road that may connect to the main road or between other branch roads, which is commonly observed in the distant regions with less sensing frequency.

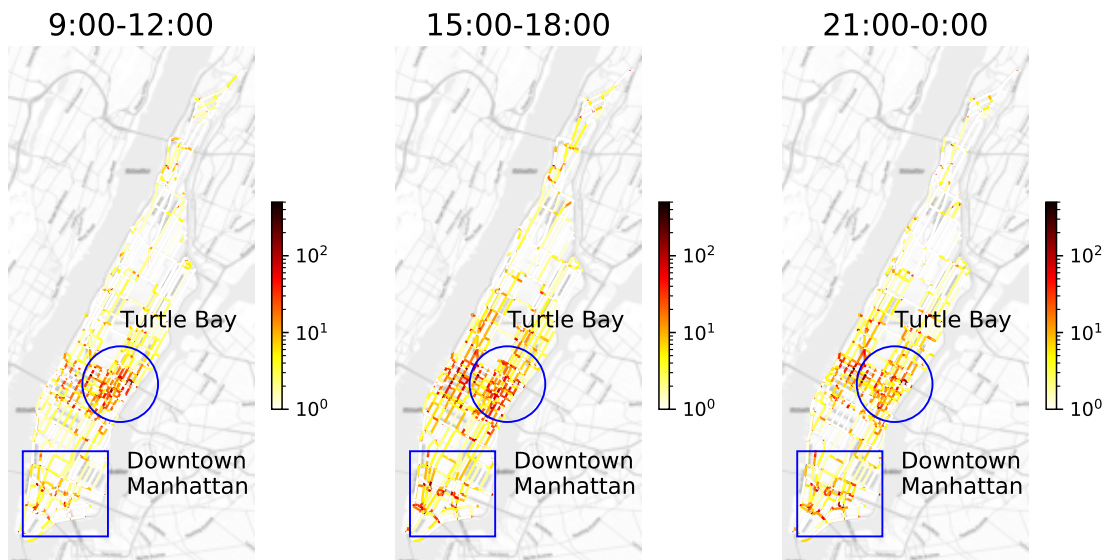


Figure 1: Spatial distribution of the RV sensing frequency (on a log scale of 10). The circled area indicates the hot spots near Turtle Bay, and the squared area is Downtown Manhattan.

From Figure 1, one immediate observation is the hot-spot areas near Turtle Bay neighborhoods (see circled areas), where certain links can attract more than 500 visits across all three-hour periods. In addition, we find that the Downtown Manhattan area (squared) serves as another hot spot, especially during 3 PM - 6 PM and 9 PM - 12 AM. It implies the extensive short-length trips of unoccupied RVs from and to Downtown Manhattan area. In these areas, the vehicles can serve

immediately available requests or find the potential passengers within a short period of waiting, yielding a higher sensing frequency. In summary, those two hot spots denote the number of visits of 16,592, 22,645, and 15,977, covering 29.3%, 21.5%, 24.0% of all visits during the three time periods.

6.2. Sensing coverage and reliability: the baseline scenario

In this subsection, we present the weekly average historical sensing performance in terms of the temporal distribution of coverage rates from 9 AM to 3 AM (the next day), sensing reliability under different fleet sizes, and the independence scores for different time periods.

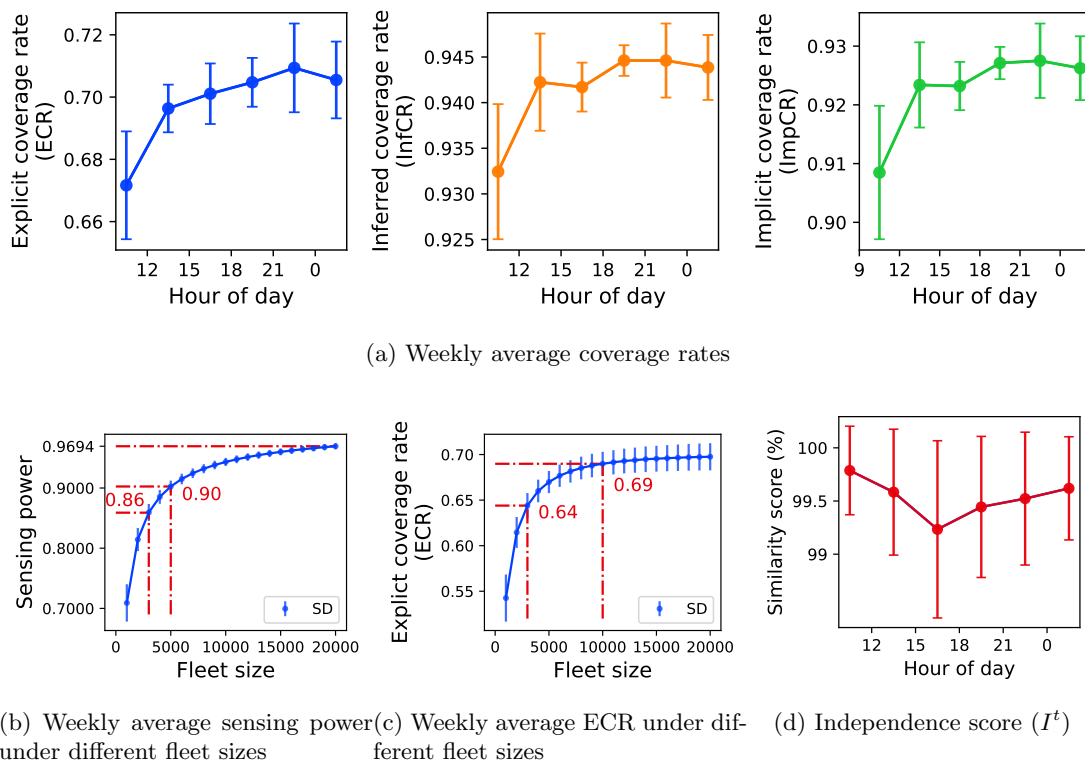


Figure 2: Distribution and coverage rate using inferred information

As seen in Figure 2a, we report that the lowest coverage rates take place in the morning periods (9 AM - 12 PM). In the morning on the weekdays, the commuters share similar OD trajectories with the relatively fixed routes, e.g., from residential areas to the workplace. However, the links in other areas are rarely visited, resulting in low ECRs. In addition, the link coverage during morning time periods may perform well on the main roads but relatively poor along the branch roads. Thus, branch roads, especially in distant regions, can hardly be inferred by considering few visits and the complexity of the road network. Analogously, the trajectories during 12 AM - 3 AM may only cover

the roads in the high-demand region, where the explicit visit will result in a lower link coverage rate, even after inferring the implicit information from the unvisited links (see the slight drops after 12 AM in Figure 2a). As for the ImpCRs, it follows similar trends as the InfCR, where both start at the lowest level at 0.932 and 0.908 at 9 AM and plateau starting at 6 PM - 9 PM. In particular, over 90.8% of the links with great inferring potential have already been traversed, hinting at the high coverage on the main roads. Additional insights are drawn into the standard deviations (SDs) along the time horizon. The afternoon and evening time period (3 PM - 9 PM) depicts more robustness, indicating relatively higher link coverage on main and branch roads. Nevertheless, two periods during the morning (9 AM - 12 PM) and midnight (12 AM - 3 AM) exhibit fluctuating coverage rates, which may be caused by varying route choices along the weekday and weekend, and in turn, the dynamic distribution of traversed road segments.

Besides the sensing coverage, we further remark on the sensing performance on the reliability, quantified by the sensing power. While our data denotes varying fleet sizes on each day, we only select the data with a fleet size over 20,000 (four days in total). And we next inspect the sensing power under fleet size from 1,000 to 20,000, step by 1,000. Since the RVs under different fleet sizes are randomly sampled from the historical data, we use ten random seeds so as to measure the average performance of the sensing power. We set 20,000 as the maximum fleet size to investigate the potential plateau of sensing power under the full fleet size.

As seen in Figure 2b, the sensing power shows minor differences over one day, where the period of 3 PM to 6 PM slightly outperforms other periods, indicating the varying destinations and more road segments being traversed. We also observe a clear marginal effect where the sensing power increases more slowly as the fleet size grows, especially with a fleet size of more than 10,000 RVs. In particular, 50 % of RVs can support a sensing power of 0.90, yielding around 93.1% of the maximum sensing power, while a sensing power of 0.86 only requires 3,000 RVs (about 15% of the fleet). Looking at the explicit coverage rate (ECR) in Figure 2c, we report that the link coverage rate approximately follows an exponential function, where 10,000 RVs (50% of the fleet) can denote an ECR of 69.0% on average. In addition, 3,000 RVs (15% of the fleet) can still support an ECR of 64.0%. As discussed in Section 4.2, the sensing power can reflect the sensing reliability of the traversed (observed) road segments by inspecting the probability of revisiting the observed roads. As presented in Figure 2c, only 5,000 RVs (25% of the RV fleet) can reach a sensing power of 0.9,

which exhibits great potential on the sensing reliability to support a stable high InfCR and ImpCR for daily operations. These metrics prove that RVs can serve as a highly effective and robust sensing solution for the surveillance of urban transportation networks under a moderate fleet size.

Further, we validate our assumption regarding the spatial- and temporal-independent trips and we present the independence score in Figure 2d. Specifically, we adopt a rolling time window of 15 minutes within a three-hour period. Then, we calculate the independence score within the 15-minute rolling time window considering the number of visits per link \mathbf{v}^t and the expected visits $\bar{\mathbf{v}}^t$ in different scenarios (e.g., time window threshold δ and the shortest-path search range K). We note that the average values suggest a high independent level of over 99.0%, and the SDs also indicate the robustness of the independence over different scenarios in different time periods.

6.3. Results of optimal rerouting strategy

We next show the improvement of sensing performance regarding sensing coverage and reliability by comparing the baseline scenario and the results of in the optimal rerouting strategy (under the scenario of $\delta = 1.0$ and $K = 20$). Specifically, we select the RV trajectory data on one weekday (April 19, 2017) covering morning, afternoon, and night time periods. For convenience, let “K-SPH” denote “K-Shortest-Path Heuristics algorithm” in Algorithm 1 and “RG” denote “Rule-based Greedy algorithm” in Algorithm 2. Also, we define three types of links, namely, unknown (U), inferred (I), and observed (O) links to better illustrate the link observability. Further, we report the detailed sensing performance, the resulted travel mileage and idling duration under different time periods (t), travel time threshold (δ), and K-shortest path search range (K). We list key metrics for sensing performance as below:

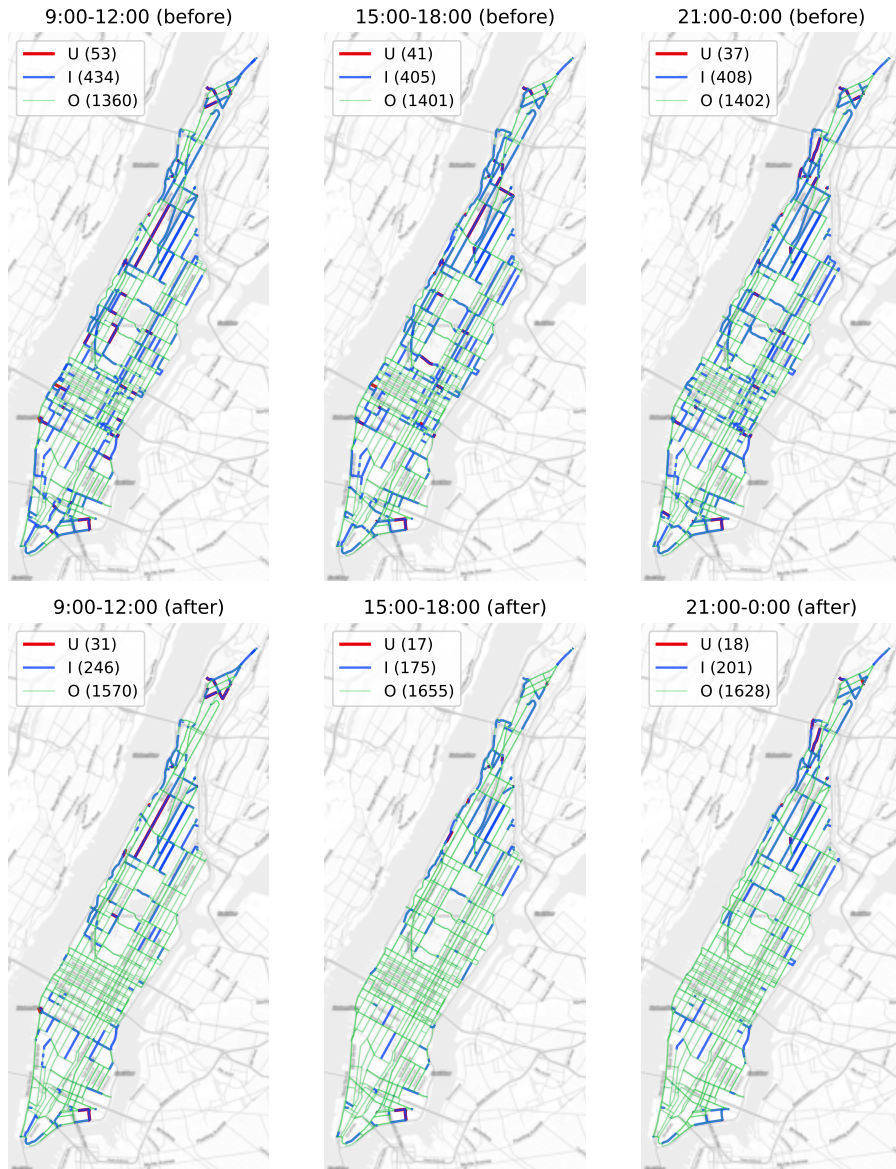
- c^{exp} : explicit coverage rate (ECR)
- c^{inf} : inferred coverage rate (InfCR)
- c^{imp} : implicit coverage rate (ImpCR)
- H^t : entropy of sensing frequency at time period t
- S^t : sensing power at time period t

- ΔD : changes of the travel distance between the optimal rerouting and the historical trajectory (positive value indicates additional travel mileage).
- ΔT : changes of idle duration between the optimal rerouting strategy and the historical trajectory (positive value indicates a prolonged idle duration).
- CPU_Time: computational time (unit: s)

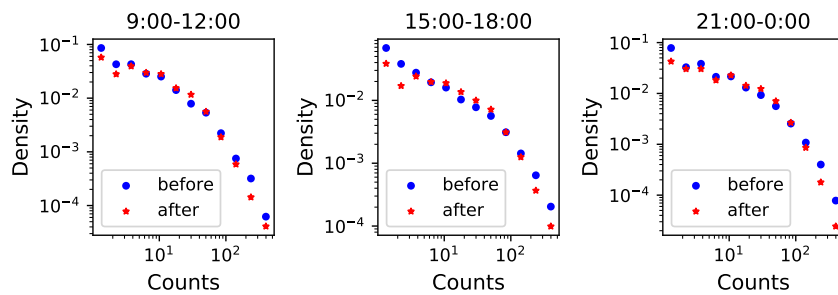
6.3.1. Comparison between optimal sensing and baseline scenario

In Figure 3a, we first show the spatial distribution of link observability in the baseline case. The selected three time periods are consistent with Figure 1. As seen in Figure 3a, we first report a high explicit coverage over the main roads, based on which the information on the branch roads can be inferred (see the blue segments between green links). In addition to a few unknown links in the Turtle Bay area, most unknown links are distributed in the Upper Manhattan area. As for the temporal changes, the time period “21:00-0:00” exhibits the most observed links (1,402) and least unknown links (37), covering 75.9% and 2.0% of all links, respectively. Such an observation is consistent with the results in Figure 1. This is potentially due to the more frequent short-length trip in the Downtown and Midtown Manhattan areas, yielding a higher number of direct visits to the links with lower sensing frequency. In addition, we also find that there is only a difference of 12 unvisited links regarding the first two time periods (53 versus 41) given different direct observations (1,360 versus 1,401). However, more links can be inferred based on the road network topology from 9 AM to 12 PM (434 versus 405). This is because the majority of visits during 9 AM - 12 PM cover the main roads, indicating a higher inferred coverage rate by inferring more branch roads in between the main roads. As such, the results suggest the potential priority of the main roads being visited, which promises possible strategies that may significantly improve the sensing performance.

After conducting the optimal rerouting, there are at most 254 additional links being directly visited after conducting the optimal rerouting. In particular, most of the links in the Middle Manhattan area are visited after rerouting. This implies that the historical cruising trips in these areas were likely to travel along repetitive routes. And our rerouting strategy motivates these RVs to traverse unobserved links and revisit the links with low visit frequency within their travel time threshold. Looking back to Upper Manhattan area, during the afternoon and evening periods (3 -



(a) Spatial distribution of sensing coverage and frequency



(b) Distribution of sensing frequency

Figure 3: Comparison between the historical records and optimal rerouting strategy on a weekday ($\delta = 1.0$, $K = 20$, U: unknown, I: inferred, O: observed.)

6 PM and 9 PM - 12 AM), we can observe that some links that are originally U and I are observed directly (O). However, the improvement in link observability after rerouting is limited, primarily due to few cruising trips in these areas, especially during late night period (9 PM - 12 AM).

Aside from the link observability, we also compare the distribution of sensing frequency during the three time periods. Before the rerouting, we report highly skewed distributions of sensing frequency, where more links are found to be visited fewer than 25 times during the three-hour period. After rerouting, we can observe a more evenly redistributed link visits as shown in the distribution curves in Figure 3b. The visiting frequency distribution after rerouting suggests that less visited links are covered more number of times as compared to the base case, as reflected by the reduced density of links with low visit counts and higher density value for links with medium number of visit counts. Moreover, there are also fewer links with high number of visits after rerouting, since RVs using repetitive paths are now redistributed to cover additional links or links with low number of visits. These trends are also observed by comparing the distribution of unknown and inferred links before and after the rerouting, where there are significantly more number of observed links and fewer unvisited links after rerouting, thus improving both explicit and implicit link coverage rate.

6.3.2. Sensitivity analyses on time window and search range

We summarize in Table 5 the specific metrics for quantifying the performances of the rerouting strategy. In the results, a larger δ allows the RV to deviate more from their original cruising path with longer travel time, and larger K may enlarge the number of candidate paths that satisfy the travel time constraint. Note that during the morning periods, the negative values of additional cruising distance indicates that the cruising distance in the optimal rerouting strategy is lower than the historical trajectory. This implies that the historical trajectory may not always follow the shortest path, yielding a longer travel distance. Meanwhile, given lower rerouting distance, we report tangible improvements in the explicit coverage and sensing power by at least 14.5% and 24.0%, respectively. As for the afternoon and night time periods, we also observe the superior performance of the optimal rerouting strategy over the base scenario before rerouting. Even the most restrictive scenario with $\delta = 0.9$ and $K = 20$ is found to improve c^{exp} by up to 17.0%, H^t by at least 4.3%, and S^t by more than 23.6%. In addition, with the rerouting strategy, up to 91.6%

Table 5: Results of the K-shortest Path-based algorithm and comparison with historical trajectory (M: Morning, 9 AM - 12 PM; A: Afternoon: 3 - 6 PM; N: Night, 9 PM - 12 AM.)

t	Scenario	δ	K	c^{exp}	c^{inf}	c^{imp}	H^t	S^t	ΔD (%)	ΔT (%)	CPU-Time
M	before	-	-	0.73	0.96	0.97	6.43	0.57	0.00	0.00	-
M	after	0.9	20	0.84	0.98	0.98	6.70	0.71	-16.84	-1.18	65.2528
M	after	0.9	40	0.84	0.98	0.98	6.72	0.71	-12.16	0.95	129.823
M	after	0.9	60	0.85	0.98	0.98	6.73	0.72	-9.74	2.05	191.025
M	after	0.9	80	0.85	0.98	0.98	6.74	0.72	-8.46	2.63	255.312
M	after	1.0	20	0.85	0.98	0.98	6.72	0.71	-11.18	1.39	70.6779
M	after	1.0	40	0.85	0.98	0.98	6.74	0.72	-5.74	3.87	141.551
M	after	1.0	60	0.86	0.98	0.98	6.75	0.73	-2.77	5.21	209.544
M	after	1.0	80	0.86	0.98	0.98	6.76	0.73	-1.07	5.99	284.286
M	after	1.1	20	0.85	0.98	0.98	6.74	0.72	-6.65	3.45	75.9069
M	after	1.1	40	0.86	0.98	0.98	6.76	0.73	-0.65	6.18	157.487
M	after	1.1	60	0.86	0.98	0.98	6.77	0.74	2.67	7.69	236.866
M	after	1.1	80	0.87	0.98	0.98	6.78	0.74	4.87	8.69	305.995
M	after	1.2	20	0.86	0.98	0.98	6.75	0.73	-2.51	5.33	79.2496
M	after	1.2	40	0.86	0.98	0.98	6.78	0.73	4.18	8.37	159.901
M	after	1.2	60	0.87	0.98	0.98	6.78	0.74	8.16	10.18	241.363
M	after	1.2	80	0.87	0.98	0.98	6.80	0.74	10.14	11.08	323.051
A	before	-	-	0.75	0.97	0.97	6.50	0.61	0.00	0.00	-
A	after	0.9	20	0.88	0.99	0.98	6.78	0.78	15.17	7.78	82.1633
A	after	0.9	40	0.89	0.99	0.98	6.80	0.79	22.89	10.43	162.323
A	after	0.9	60	0.90	0.99	0.98	6.81	0.79	26.28	11.58	245.612
A	after	0.9	80	0.90	0.99	0.98	6.81	0.79	28.98	12.51	330.427
A	after	1.0	20	0.89	0.99	0.99	6.79	0.78	22.16	10.18	88.6035
A	after	1.0	40	0.90	0.99	0.99	6.81	0.79	29.87	12.81	177.621
A	after	1.0	60	0.90	0.99	0.99	6.82	0.80	34.43	14.38	268.428
A	after	1.0	80	0.91	0.99	0.99	6.83	0.80	37.34	15.37	360.601
A	after	1.1	20	0.89	0.99	0.99	6.81	0.79	27.67	12.06	93.7939
A	after	1.1	40	0.90	0.99	0.99	6.83	0.80	35.64	14.79	189.246
A	after	1.1	60	0.91	0.99	0.99	6.84	0.80	41.02	16.63	286.926
A	after	1.1	80	0.91	0.99	0.99	6.84	0.81	44.05	17.67	383.507
A	after	1.2	20	0.90	0.99	0.99	6.82	0.79	31.52	13.38	98.1889
A	after	1.2	40	0.91	0.99	0.99	6.84	0.81	41.23	16.71	199
A	after	1.2	60	0.91	0.99	0.99	6.85	0.81	46.88	18.64	304.302
A	after	1.2	80	0.92	0.99	0.99	6.86	0.81	50.46	19.87	408.394
N	before	-	-	0.76	0.97	0.98	6.49	0.64	0.00	0.00	-
N	after	0.9	20	0.88	0.99	0.99	6.82	0.79	9.94	7.42	92.5123
N	after	0.9	40	0.88	0.99	0.98	6.84	0.80	15.77	9.35	183.61
N	after	0.9	60	0.88	0.99	0.99	6.85	0.80	17.97	10.07	270.461
N	after	0.9	80	0.88	0.99	0.99	6.86	0.80	19.70	10.65	356.857
N	after	1.0	20	0.88	0.99	0.99	6.84	0.79	16.33	9.53	99.1783
N	after	1.0	40	0.89	0.99	0.98	6.86	0.80	23.35	11.85	197.568
N	after	1.0	60	0.89	0.99	0.99	6.87	0.81	26.49	12.89	292.708
N	after	1.0	80	0.89	0.99	0.99	6.87	0.81	27.76	13.31	385.97
N	after	1.1	20	0.89	0.99	0.99	6.86	0.80	22.07	11.43	106.658
N	after	1.1	40	0.89	0.99	0.99	6.88	0.81	31.09	14.41	211.697
N	after	1.1	60	0.89	0.99	0.99	6.89	0.81	34.40	15.50	314.583
N	after	1.1	80	0.90	0.99	0.99	6.90	0.82	37.38	16.48	413.813
N	after	1.2	20	0.89	0.99	0.99	6.88	0.81	27.99	13.38	114.186
N	after	1.2	40	0.89	0.99	0.99	6.90	0.82	37.71	16.59	225.387
N	after	1.2	60	0.90	0.99	0.99	6.91	0.82	41.22	17.75	335.631
N	after	1.2	80	0.90	0.99	0.99	6.92	0.82	44.36	18.79	446.487

of the road segments can be immediately observed and over 99.1% of the road segments can be observed and inferred. This reflects the significant potential for optimally advising the cruising trips of RVs so that information on less visited links can either be directly probed or indirectly inferred for improved sensing coverage. And a close to 100% coverage is admissible with the current RV capacity without sacrificing its level of service.

Moreover, with the same fleet size, the greater sensing coverage can be achieved along with a significantly improved sensing reliability as captured by S^t . Specifically, the sensing power is found to increase by up to 30.8%, 32.7%, and 28.4% during morning, afternoon, and night time periods, representing more reliable sensing performances in certain time intervals. The improved sensing power indicates that the same sensing coverage are more likely to be achieved on a daily basis, which highlights the practical value of using RVs to monitor the urban road network. The improved sensing coverage and sensing reliability will allow for high quality and more robust data analytic jobs for smart city applications such as travel time prediction, fuel consumption analyses, and air quality monitoring. More importantly, the sensing performances of RVs also have significant implications for the development of autonomous driving vehicles. In this case, more visited road segments and reliable visiting dynamics across various time periods will deliver consistent and diverse driving data for training purposes.

We also present in Figure 4 the results of the rule-based greedy algorithm (RG) in comparison with the results of the K-shortest path algorithm (K-SPH) and the baseline scenario. More detailed results of RG are shown in Appendix Table B.7. We report that even the worst sensing performance in K-SPH is superior to the best performance in RG during all three time periods. For instance, during 9 PM - 12 AM, the best ECR and sensing power is 0.857 and 0.723 under $\delta = 1.2$, which are still 2.1% and 8.5% lower than the most restrictive scenario in K-SPH ($\delta = 0.9, K = 20$). As for the travel distance and idle duration, all scenarios are associated with savings of mileage in the rerouting trips and prolonged idling duration than the historical baseline and the results of K-SPH. This is because the RG myopically selects the shortest path with the least sensing frequency. In this case, an RV is likely to be assigned to a short-length trip that locally traverses the road segments with fewer visits. Also, the RV may finish the rerouting trip within a short time period and wait for the next request, resulting in a longer idle duration. On the contrary, K-SPH focuses globally on the entropy of sensing frequency. An RV following K-SPH may deviate more from the original

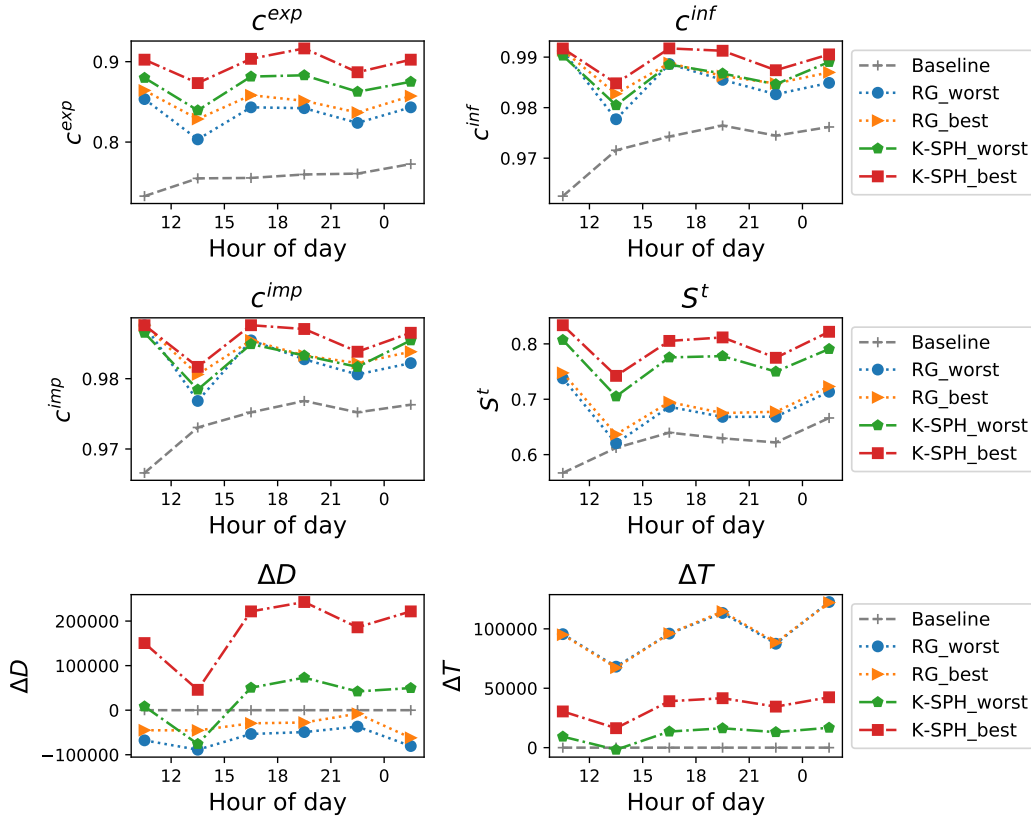


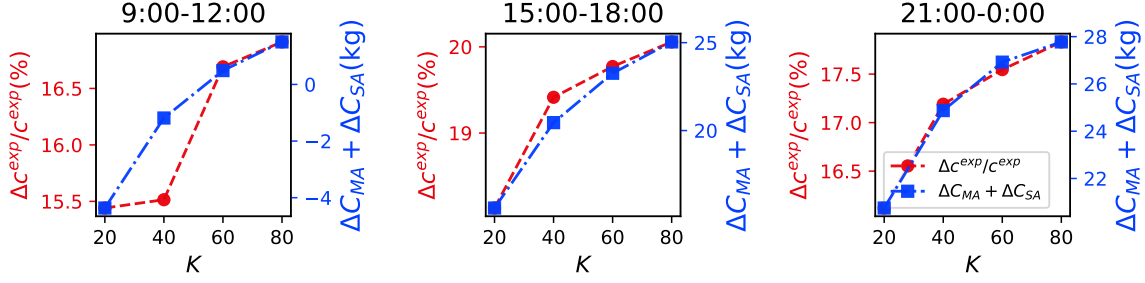
Figure 4: Comparison between RG, K-SPH and historical baseline.

path to achieve a higher entropy within the time window constraint.

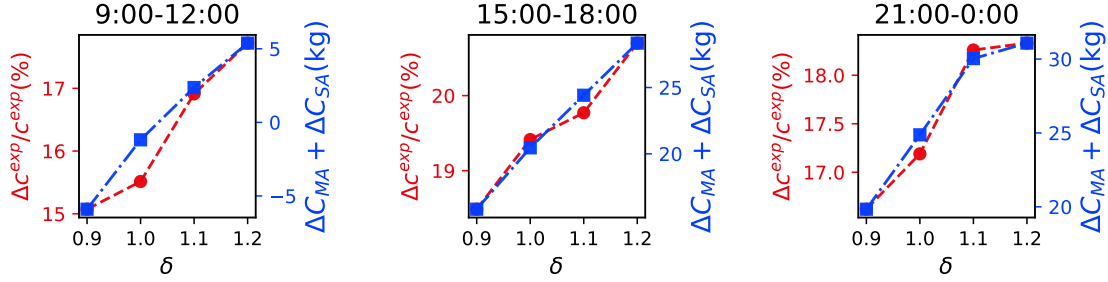
Further, we observe that the RG requires a significantly short computation time (less than 5 seconds) than the K-SPH. This indicates that the computational efforts for K-SPH are mostly for searching the K shortest path and selecting the one that can most contribute to the entropy of sensing frequency. By compromising more computational efforts, superior sensing performance can be achieved in K-SPH. For the practical scenario, we note that the computation time for the K-SPH is permissible if the unoccupied RVs proceed sequentially within a broader time period. Considering the number of unoccupied RVs (at least 1,000 RVs per three-hour time period), we report that the optimal rerouting trajectory can be generated in less than 1 second, which is applicable for a real-time assignment.

6.3.3. Sensitivity analyses on fuel consumption and emission

Finally, we present the results of sensitivity analyses on fuel consumption in Figure 5 and emissions in Figure 6.



(a) Sensitivity analyses on K under the fixed $\delta = 1.0$

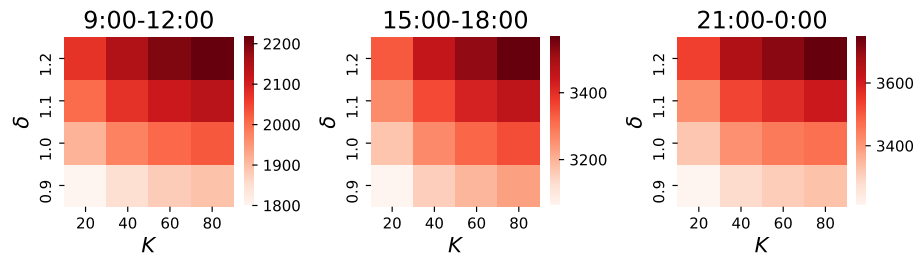


(b) Sensitivity analyses on δ under the fixed $K = 40$

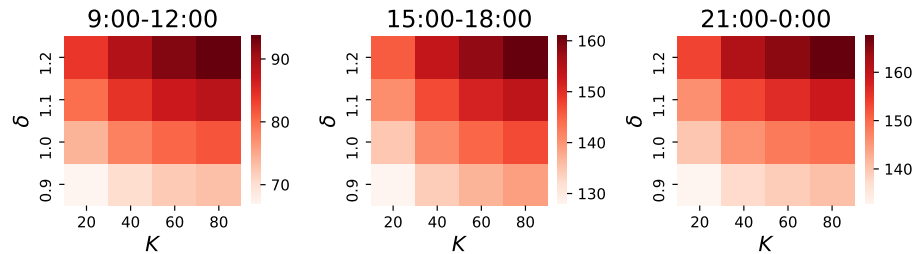
Figure 5: Trade off between improvement of ECR $\Delta C^{exp}/C^{exp}$ and additional fuel consumption $\Delta C_{MA} + \Delta C_{SA}$.

Figure 5 displays the trade-off between the improvement in ECR and the increment of fuel consumption following the optimal rerouting strategy. In general, with a larger search range K or less restrictive time threshold δ , the ECRs are observed to increase by at least 1.5%. Meanwhile, it incurs additional fuel consumption of up to 15 kg. In addition, the improvements in ECR are found to be marginal with larger K as shown in Figure 5a. The same observation holds for the fuel consumption with a larger K . This indicates that the optimal routes are sufficiently covered by searching up to 60 shortest paths, and further routes can hardly meet the travel time constraint. However, as seen in Figure 5b, the ECR and fuel consumption are found to increase linearly with δ under the same $K = 40$ during all three time periods (except the case with $\delta = 1.2$ during 9 PM - 12 AM). As such, it suggests that a relaxed travel time threshold contributes more than a wider search range of shortest-path regarding the improvement of sensing performance. Further, under a relaxed time threshold from 0.9 to 1.2, we report that the largest improvement in ECR is during 9 AM - 12 PM (up to 2.64%) with the an increment of fuel consumption of 11.29 kg. Meanwhile, the other two time periods, 3 - 6 PM and 9 PM - 12 AM, denote an improvement in ECR of 2.21% and 1.71% with additional fuel consumption of 12.53 kg and 11.24 kg, respectively. The highest

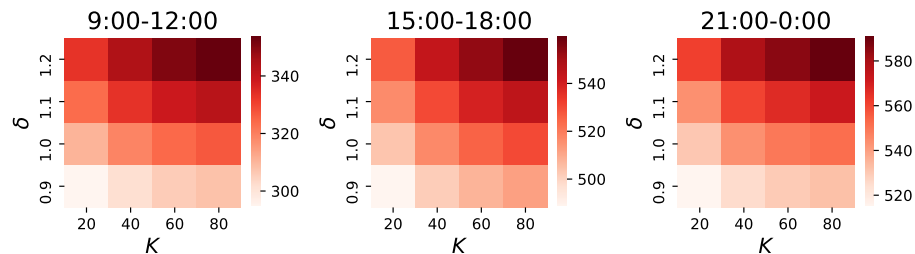
increase in ECR indicates great potential of the rerouting strategy. Especially during the morning period, given a good sensing coverage of main roads (see Figure 3a), one may only need to slightly deviate from the original path to traverse the road segments in need (e.g., the branch roads nearby). Also, during the morning period, our optimal rerouting strategy can increase the ECR by at least 15.5% under $\delta = 1.0$ and $K = 40$ with no additional fuel consumption, which suggests an effective rerouting solution for the sensing task in practice.



(a) Additional emission factor of CO (unit: g)



(b) Additional emission factor of NO_x (unit: g)



(c) Additional emission factor of HC (unit: g)

Figure 6: Sensitivity analyses during three time periods under different travel time thresholds (δ) and search ranges of shortest path (K).

We next focus on the emission factors regarding CO, NO_x , and HC. Similar to the observation on fuel consumption, higher emissions are found with more relaxed scenarios (e.g., larger K and δ). This is because, under a relaxed scenario, one RV is more likely to make a significant detour that contributes most to the sensing performance while still satisfying the time window constraint.

However, such a significant detour may be infeasible due to the time limit, resulting in a relatively short trip and thus lower emissions. In addition, we note the increment of all three emission factors is found to be the lowest in the morning period than in the other two time periods. Specifically, the emissions of CO, NO_x, and HC during the morning period are 17.3%, 19.0%, and 16.8% lower than the afternoon period and 22.4%, 23.1%, and 22.2% lower than night period, respectively. Combining with the most remarkable improvement in ECR during the morning period (shown in Figure 5b), such lowest increments in emission factors indicate that a minor adjustment on the original trajectory can lead to a significant improvement in sensing performance. One particular case is the most restrictive case $\delta = 0.9, K = 20$ in the morning period, where the additional emissions are observed, but both ΔD and ΔT are negative. This is potentially due to the difference in speed (v_{ij}) such that higher emissions may exist in some road segments even though the total mileage and idle duration are reduced/prolonged than the historical baseline.

7. Conclusion

This study investigates a novel approach to deploying ridesourcing vehicles for drive-by sensing in a large-scale urban road network. We first investigate the historical sensing performance regarding explicit coverage rate and sensing reliability. Based on that, we explore the potential inferable information on the unvisited road segments given explicit observations and network topology. We further propose the optimal rerouting strategy that guides the unoccupied RVs to cruise along with specific unvisited links and to revisit the links with relatively low sensing frequency with a particular focus on the sensing coverage and sensing reliability. The optimal rerouting strategy is formulated as an entropy maximization problem, and we prove that the optimal solution can simultaneously maximize the explicit coverage rate and sensing power, thus reinforcing the sensing performance. To solve the entropy maximization problem, we develop one heuristic algorithm, which can provide high-quality rerouting paths to a sequence of unoccupied RVs in real-time. The results show that while only 75.5% of road segments are explicitly traversed by RVs, over 97.2% of road network information can be inferred from the actual observations, and only less than 1% of additional links need to be visited in order to reach the 100% network coverage rate. Besides, our optimal rerouting strategy demonstrates superior performance on both sensing coverage and reliability, which has improved the ECR by at least 31.1% and the sensing power by up to 32.7%. Sensitivity analyses

reveal that less restrictive time constraints and a larger search range of shortest path contribute to the sensing coverage by up to 20.6%. In particular, an increase of 15.5% in ECR can be achieved with no additional fuel consumption, suggesting a cost-effective solution to enhance the sensing performance in practice. Finally, we note that the fleet deployment for sensing may individually sacrifice the driver income but will achieve an overall high performance on the link coverage, and the results imply a promising direction for coordinated operation of connected and autonomous RVs considering the network sensing as a subtask of their daily operations.

References

- S. Abdelhamid, H. S. Hassanein, and G. Takahara. Vehicle as a mobile sensor. *Procedia Computer Science*, 34:286–295, 2014.
- S. Abdelhamid, H. S. Hassanein, and G. Takahara. Vehicle as a resource (vaar). *IEEE Network*, 29(1):12–17, 2015.
- M. Abramowitz, I. A. Stegun, and R. H. Romer. Handbook of mathematical functions with formulas, graphs, and mathematical tables, 1988.
- D. Agarwal, S. Iyengar, M. Swaminathan, E. Sharma, A. Raj, and A. Hatwar. Modulo: Drive-by sensing at city-scale on the cheap. In *Proceedings of the 3rd ACM SIGCAS Conference on Computing and Sustainable Societies*, pages 187–197, 2020.
- R. K. Ahuja, T. L. Magnanti, and J. B. Orlin. Network flows. Technical report, DTIC Document, 1988.
- A. Anjomshoaa, F. Duarte, D. Rennings, T. J. Matarazzo, P. deSouza, and C. Ratti. City scanner: Building and scheduling a mobile sensing platform for smart city services. *IEEE Internet of things Journal*, 5(6):4567–4579, 2018.
- A. Anjomshoaa, P. Santi, F. Duarte, and C. Ratti. Quantifying the spatio-temporal potential of drive-by sensing in smart cities. *Journal of Urban Technology*, pages 1–18, 2020.
- X. Ban, Y. Li, A. Skabardonis, and J.-D. Margulici. Performance evaluation of travel time methods for real time traffic applications. In *11th World Conference on Transport Research*, 2007.
- X. J. Ban, R. Herring, J. Margulici, and A. M. Bayen. Optimal sensor placement for freeway travel time estimation. In *Transportation and traffic theory 2009: Golden jubilee*, pages 697–721. Springer, 2009.
- G. Boeing. Osmnx: New methods for acquiring, constructing, analyzing, and visualizing complex street networks. *Computers, Environment and Urban Systems*, 65:126–139, 2017.

- Z. Cui, K. Henrickson, R. Ke, and Y. Wang. Traffic graph convolutional recurrent neural network: A deep learning framework for network-scale traffic learning and forecasting. *IEEE Transactions on Intelligent Transportation Systems*, 21(11):4883–4894, 2019.
- P. Desouza, A. Anjomshoaa, F. Duarte, R. Kahn, P. Kumar, and C. Ratti. Air quality monitoring using mobile low-cost sensors mounted on trash-trucks: Methods development and lessons learned. *Sustainable Cities and Society*, 60:102239, 2020.
- X. Fei, H. S. Mahmassani, and S. M. Eisenman. Sensor coverage and location for real-time traffic prediction in large-scale networks. *Transportation Research Record*, 2039(1):1–15, 2007.
- X. Fei, H. S. Mahmassani, and P. Murray-Tuite. Vehicular network sensor placement optimization under uncertainty. *Transportation Research Part C: Emerging Technologies*, 29:14–31, 2013.
- I. Fujito, R. Margiotta, W. Huang, and W. A. Perez. Effect of sensor spacing on performance measure calculations. *Transportation research record*, 1945(1):1–11, 2006.
- M. Gentili and P. B. Mirchandani. Review of optimal sensor location models for travel time estimation. *Transportation Research Part C: Emerging Technologies*, 90:74–96, 2018.
- S. Guo, X. Qian, S. Dasgupta, M. Rahman, and S. Jones. Sensing and monitoring of urban roadway traffic state with large-scale ride-sourcing vehicles. *The Rise of Smart Cities*, pages 551–582, 2022.
- S.-x. He. A graphical approach to identify sensor locations for link flow inference. *Transportation Research Part B: Methodological*, 51:65–76, 2013.
- J. C. Herrera, D. B. Work, R. Herring, X. J. Ban, Q. Jacobson, and A. M. Bayen. Evaluation of traffic data obtained via gps-enabled mobile phones: The mobile century field experiment. *Transportation Research Part C: Emerging Technologies*, 18(4):568–583, 2010.
- S.-R. Hu, S. Peeta, and C.-H. Chu. Identification of vehicle sensor locations for link-based network traffic applications. *Transportation Research Part B: Methodological*, 43(8-9):873–894, 2009.
- S. M. Khan, S. Atamturktur, M. Chowdhury, and M. Rahman. Integration of structural health monitoring and intelligent transportation systems for bridge condition assessment: current status and future direction. *IEEE Transactions on Intelligent Transportation Systems*, 17(8):2107–2122, 2016.
- W. Lam and H. Lo. Accuracy of od estimates from traffic counts. *Traffic engineering & control*, 31(6), 1990.
- X. Li and Y. Ouyang. Reliable sensor deployment for network traffic surveillance. *Transportation research part B: methodological*, 45(1):218–231, 2011.
- D. Luxen and C. Vetter. Real-time routing with openstreetmap data. In *Proceedings of the 19th ACM SIGSPATIAL International Conference on Advances in Geographic Information Systems*, GIS '11,

- pages 513–516, New York, NY, USA, 2011. ACM. ISBN 978-1-4503-1031-4. doi: 10.1145/2093973.2094062. URL <http://doi.acm.org/10.1145/2093973.2094062>.
- W. Ma and S. Qian. High-resolution traffic sensing with probe autonomous vehicles: A data-driven approach. *Sensors*, 21(2):464, 2021.
- S. Mora, A. Anjomshoaa, T. Benson, F. Duarte, and C. Ratti. Towards large-scale drive-by sensing with multi-purpose city scanner nodes. In *2019 IEEE 5th World Forum on Internet of Things (WF-IoT)*, pages 743–748. IEEE, 2019.
- M. Ng. Synergistic sensor location for link flow inference without path enumeration: A node-based approach. *Transportation Research Part B: Methodological*, 46(6):781–788, 2012.
- L. Ntziachristos, D. Gkatzoflias, C. Kouridis, and Z. Samaras. Copert: a european road transport emission inventory model. In *Information technologies in environmental engineering*, pages 491–504. Springer, 2009.
- NYCTLC. Tlc factbook. <https://www1.nyc.gov/assets/tlc/downloads/pdf/2020-tlc-factbook.pdf>, 2021. Accessed on May 2022.
- OpenStreetMap contributors. Planet dump retrieved from <https://planet.osm.org> . <https://www.openstreetmap.org>, 2017.
- K. P. O’Keeffe, A. Anjomshoaa, S. H. Strogatz, P. Santi, and C. Ratti. Quantifying the sensing power of vehicle fleets. *Proceedings of the National Academy of Sciences*, 116(26):12752–12757, 2019.
- H. Park and A. Haghani. Optimal number and location of bluetooth sensors considering stochastic travel time prediction. *Transportation Research Part C: Emerging Technologies*, 55:203–216, 2015.
- X. Qian, X. Zhan, and S. V. Ukkusuri. Characterizing urban dynamics using large scale taxicab data. In *Engineering and Applied Sciences Optimization*, pages 17–32. Springer, 2015.
- X. Qian, D. Kumar, W. Zhang, and S. V. Ukkusuri. Understanding the operational dynamics of mobility service providers: A case of uber. *ACM Transactions on Spatial Algorithms and Systems (TSAS)*, 6(2):1–20, 2020a.
- X. Qian, T. Lei, J. Xue, Z. Lei, and S. V. Ukkusuri. Impact of transportation network companies on urban congestion: Evidence from large-scale trajectory data. *Sustainable Cities and Society*, 55:102053, 2020b.
- X. Qian, S. V. Ukkusuri, C. Yang, and F. Yan. Short-term demand forecasting for on-demand mobility service. *IEEE Transactions on Intelligent Transportation Systems*, 2020c.
- M. M. Solomon. Algorithms for the vehicle routing and scheduling problems with time window constraints. *Operations research*, 35(2):254–265, 1987.

- Z. Sun and X. J. Ban. Vehicle trajectory reconstruction for signalized intersections using mobile traffic sensors. *Transportation Research Part C: Emerging Technologies*, 36:268–283, 2013.
- F. Viti, M. Rinaldi, F. Corman, and C. M. Tampère. Assessing partial observability in network sensor location problems. *Transportation research part B: methodological*, 70:65–89, 2014.
- D. B. Work, O.-P. Tossavainen, S. Blandin, A. M. Bayen, T. Iwuchukwu, and K. Tracton. An ensemble kalman filtering approach to highway traffic estimation using gps enabled mobile devices. In *2008 47th IEEE Conference on Decision and Control*, pages 5062–5068. IEEE, 2008.
- X. Xu, H. K. Lo, A. Chen, and E. Castillo. Robust network sensor location for complete link flow observability under uncertainty. *Transportation Research Part B: Methodological*, 88:1–20, 2016.
- H. Yang and J. Zhou. Optimal traffic counting locations for origin–destination matrix estimation. *Transportation Research Part B: Methodological*, 32(2):109–126, 1998.
- H. Yang, Y. Iida, and T. Sasaki. An analysis of the reliability of an origin-destination trip matrix estimated from traffic counts. *Transportation Research Part B: Methodological*, 25(5):351–363, 1991.
- J. Y. Yen. Finding the k shortest loopless paths in a network. *management Science*, 17(11):712–716, 1971.
- J. Yoon, B. Noble, and M. Liu. Surface street traffic estimation. In *Proceedings of the 5th international conference on Mobile systems, applications and services*, pages 220–232, 2007.
- X. Zhou and G. F. List. An information-theoretic sensor location model for traffic origin-destination demand estimation applications. *Transportation Science*, 44(2):254–273, 2010.

Appendix A. Proof of proposition 1

Proposition 1 *Suppose \mathbf{R}^* is the optimal solution to the maximization of H^t in Eq. (9)), then \mathbf{R}^* is also the optimal solution to the maximization of the sensing power in Eq. (7).*

Proof. Without loss of generality, we formulate the objective in Eq. (9) as a maximum entropy problem under the constraint $\sum_{(i,j) \in \mathcal{A}} P_{ij}^t = 1, \forall t \in \mathcal{T}$, since both problems have the same feasible region. For simplicity, we express P_{ij} in replace of $P_{ij}^t, t \in \mathcal{T}$ in the following proof. We solve the constrained optimization using Lagrangian relaxation with multiplier λ , which can be expressed as:

$$\mathcal{L}(P_{i,j}, \lambda) = - \sum_{(i,j) \in \mathcal{A}} P_{ij} \log P_{ij} + \lambda \left(1 - \sum_{(i,j) \in \mathcal{A}} P_{ij} \right) \quad (\text{A.1})$$

Then we have the partial derivatives as below:

$$\frac{\partial \mathcal{L}}{\partial P_{ij}} = -\log P_{ij} - 1 - \lambda \quad (\text{A.2})$$

$$\frac{\partial \mathcal{L}}{\partial \lambda} = - \left(1 - \sum_{(i,j) \in \mathcal{A}} P_{ij} \right) \quad (\text{A.3})$$

Following the first-order necessary condition, let the partial derivatives $\frac{\partial \mathcal{L}}{\partial P_{ij}} = 0$ and $\frac{\partial \mathcal{L}}{\partial \lambda} = 0$.

Then we have:

$$P_{ij} = \frac{1}{|\mathcal{A}|} = \exp(-1 - \lambda) \quad (\text{A.4})$$

Hence, the maximum entropy is achieved when P_{ij} follows the uniform distribution.

We will next show that the same condition holds for maximizing the sensing power in Eq. (7), where the sensing frequency $P_{ij} = \frac{1}{|\mathcal{A}|}, (i, j) \in \mathcal{A}$. Given each component P_{ij} are non-negative, we can reformulate it following the geometric-mean inequality, which takes the form:

$$1 - \frac{1}{|\mathcal{A}|} \sum_{(i,j) \in \mathcal{A}} (1 - P_{ij})^{|\mathcal{R}^t|} \leq 1 - \left(\prod_{(i,j) \in \mathcal{A}} (1 - P_{ij})^{|\mathcal{R}^t|} \right)^{\frac{1}{|\mathcal{A}|}} \quad (\text{A.5})$$

$$= 1 - \left(\prod_{(i,j) \in \mathcal{A}} (1 - P_{ij}) \right)^{\frac{|\mathcal{R}^t|}{|\mathcal{A}|}} \quad (\text{A.6})$$

where the equality in Eq. (A.5) holds if and only if each component $(1 - P_{ij})$ is equal (Abramowitz et al. 1988). Recalling that P_{ij} is the sensing frequency and $\sum_{(i,j) \in \mathcal{A}} P_{ij} = 1$, we therefore have $P_{ij} = \frac{1}{|\mathcal{A}|}$, which indicates the same optimal solution in Eq. (A.4). \square

Appendix B. Detailed results

Appendix B.1. Results for other time periods in Figure 1

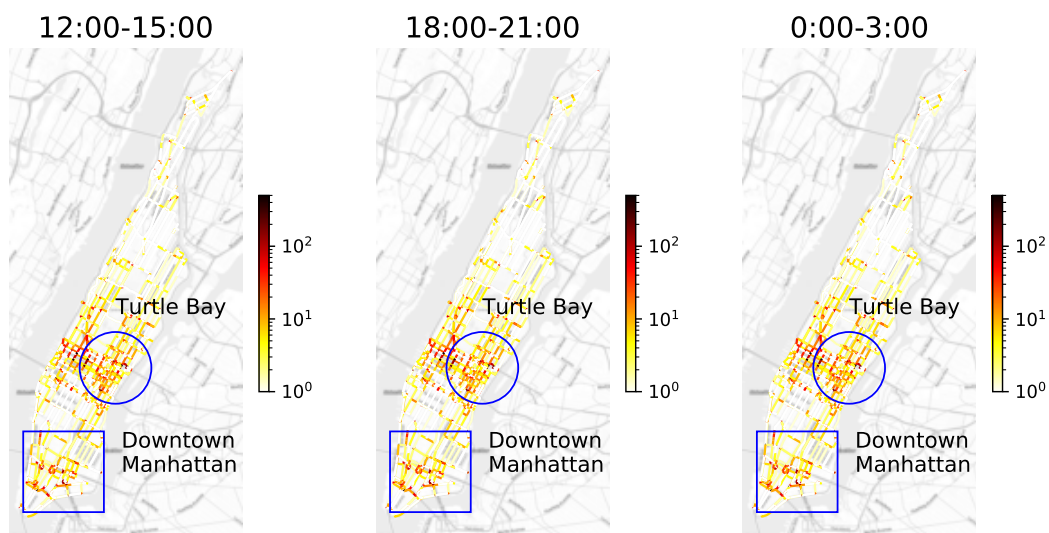


Figure B.7: Spatial distribution of the RV visit frequency (on a log scale of 10). The circled region indicates the hot spots near Turtle Bay.

Appendix B.2. Detailed results for Algorithm 1 in other time periods

Table B.6: Results of the K-shortest Path-based algorithm and comparison with historical trajectory

t	Scenario	δ	K	c^{exp}	c^{inf}	c^{imp}	H^t	S^t	ΔD	ΔT	CPU_Time
12 PM - 3 PM	before	-	-	0.76	0.98	0.98	6.59	0.63	0.00	0.00	-
12 PM - 3 PM	after	0.9	20	0.88	0.99	0.98	6.84	0.78	11.02	7.62	80.2265
12 PM - 3 PM	after	0.9	40	0.88	0.99	0.98	6.85	0.78	16.85	9.86	157.308
12 PM - 3 PM	after	0.9	60	0.89	0.99	0.99	6.86	0.78	19.34	10.81	235.039
12 PM - 3 PM	after	0.9	80	0.89	0.99	0.99	6.86	0.78	21.40	11.60	311.446
12 PM - 3 PM	after	1.0	20	0.89	0.99	0.99	6.86	0.78	18.13	10.35	87.2639
12 PM - 3 PM	after	1.0	40	0.89	0.99	0.99	6.87	0.79	24.31	12.72	170.216
12 PM - 3 PM	after	1.0	60	0.89	0.99	0.99	6.88	0.79	27.12	13.80	255.065
12 PM - 3 PM	after	1.0	80	0.89	0.99	0.99	6.88	0.79	29.93	14.88	334.361
12 PM - 3 PM	after	1.1	20	0.89	0.99	0.99	6.88	0.79	27.06	13.78	94.8827
12 PM - 3 PM	after	1.1	40	0.90	0.99	0.99	6.89	0.80	33.94	16.41	187.568
12 PM - 3 PM	after	1.1	60	0.90	0.99	0.99	6.90	0.80	37.71	17.86	275.977
12 PM - 3 PM	after	1.1	80	0.90	0.99	0.99	6.90	0.80	40.63	18.98	363.788
12 PM - 3 PM	after	1.2	20	0.90	0.99	0.99	6.89	0.79	33.42	16.22	101.53
12 PM - 3 PM	after	1.2	40	0.90	0.99	0.99	6.91	0.80	40.27	18.84	200.396
12 PM - 3 PM	after	1.2	60	0.90	0.99	0.99	6.92	0.81	44.86	20.61	301.035
12 PM - 3 PM	after	1.2	80	0.90	0.99	0.99	6.92	0.81	48.50	22.00	399.697
6 PM - 9 PM	before	-	-	0.76	0.97	0.98	6.56	0.62	0.00	0.00	-
6 PM - 9 PM	after	0.9	20	0.86	0.98	0.98	6.79	0.75	10.24	7.47	81.7234
6 PM - 9 PM	after	0.9	40	0.87	0.98	0.98	6.81	0.76	16.75	9.75	160.135
6 PM - 9 PM	after	0.9	60	0.87	0.98	0.98	6.82	0.76	20.44	11.03	241.639
6 PM - 9 PM	after	0.9	80	0.87	0.99	0.98	6.82	0.76	22.45	11.74	321.342
6 PM - 9 PM	after	1.0	20	0.87	0.99	0.98	6.80	0.76	16.23	9.56	87.8938
6 PM - 9 PM	after	1.0	40	0.87	0.99	0.98	6.82	0.76	23.25	12.02	172.902
6 PM - 9 PM	after	1.0	60	0.88	0.99	0.98	6.83	0.77	26.99	13.32	256.728
6 PM - 9 PM	after	1.0	80	0.88	0.99	0.98	6.84	0.77	30.22	14.45	343.103
6 PM - 9 PM	after	1.1	20	0.88	0.99	0.98	6.81	0.76	20.46	11.04	91.6479
6 PM - 9 PM	after	1.1	40	0.88	0.99	0.98	6.83	0.77	28.40	13.82	184.082
6 PM - 9 PM	after	1.1	60	0.88	0.99	0.98	6.84	0.77	32.43	15.23	274.42
6 PM - 9 PM	after	1.1	80	0.88	0.99	0.98	6.84	0.77	35.77	16.39	364.028
6 PM - 9 PM	after	1.2	20	0.88	0.99	0.98	6.82	0.76	27.38	13.46	95.9781
6 PM - 9 PM	after	1.2	40	0.88	0.99	0.98	6.84	0.77	36.68	16.71	195.263
6 PM - 9 PM	after	1.2	60	0.88	0.99	0.98	6.85	0.77	41.67	18.45	297.134
6 PM - 9 PM	after	1.2	80	0.89	0.99	0.98	6.86	0.77	45.31	19.73	392.449
12 AM - 3 AM	before	-	-	0.77	0.98	0.98	6.59	0.67	0.00	0.00	-
12 AM - 3 AM	after	0.9	20	0.88	0.99	0.99	6.85	0.81	1.62	4.86	78.8375
12 AM - 3 AM	after	0.9	40	0.89	0.99	0.99	6.87	0.82	6.10	6.70	156.135
12 AM - 3 AM	after	0.9	60	0.89	0.99	0.99	6.88	0.82	8.48	7.67	235.338
12 AM - 3 AM	after	0.9	80	0.89	0.99	0.99	6.88	0.82	10.18	8.36	316.346
12 AM - 3 AM	after	1.0	20	0.89	0.99	0.99	6.87	0.81	4.92	6.21	86.2964
12 AM - 3 AM	after	1.0	40	0.89	0.99	0.99	6.89	0.82	11.01	8.70	169.562
12 AM - 3 AM	after	1.0	60	0.89	0.99	0.99	6.89	0.82	13.45	9.70	255.515
12 AM - 3 AM	after	1.0	80	0.89	0.99	0.99	6.89	0.82	15.15	10.40	342.193
12 AM - 3 AM	after	1.1	20	0.89	0.99	0.99	6.88	0.82	11.03	8.71	92.9921
12 AM - 3 AM	after	1.1	40	0.90	0.99	0.99	6.90	0.83	17.51	11.36	182.367
12 AM - 3 AM	after	1.1	60	0.89	0.99	0.99	6.91	0.83	20.06	12.40	274.834
12 AM - 3 AM	after	1.1	80	0.90	0.99	0.99	6.91	0.83	22.14	13.25	368.361
12 AM - 3 AM	after	1.2	20	0.90	0.99	0.99	6.90	0.82	15.82	10.67	98.9409
12 AM - 3 AM	after	1.2	40	0.90	0.99	0.99	6.91	0.83	22.89	13.56	196.371
12 AM - 3 AM	after	1.2	60	0.90	0.99	0.99	6.92	0.83	26.46	15.02	295.777
12 AM - 3 AM	after	1.2	80	0.90	0.99	0.99	6.93	0.83	28.82	15.98	393.446

Appendix B.3. Detailed results for Algorithm 2

Table B.7: Results of the rule-based algorithm and comparison with historical trajectory

t	Scenario	δ	K	c^{exp}	c^{inf}	c^{imp}	H^t	S^t	ΔD	ΔT	CPU_Time
9 AM - 12 PM	before	-	-	0.733	0.962	0.967	6.434	0.567	0.00	0.00	-
9 AM - 12 PM	after	0.9	1	0.803	0.978	0.977	6.441	0.621	-19.69	46.10	2.0
9 AM - 12 PM	after	1.0	1	0.805	0.978	0.977	6.445	0.623	-19.16	46.15	2.0
9 AM - 12 PM	after	1.1	1	0.823	0.981	0.979	6.456	0.631	-14.33	45.96	2.0
9 AM - 12 PM	after	1.2	1	0.829	0.983	0.981	6.463	0.636	-10.08	45.50	2.0
12 PM - 3 PM	before	-	-	0.760	0.976	0.977	6.594	0.629	0.00	0.00	-
12 PM - 3 PM	after	0.9	1	0.843	0.989	0.985	6.611	0.686	-11.69	54.01	2.4
12 PM - 3 PM	after	1.0	1	0.850	0.989	0.985	6.616	0.690	-9.47	54.20	2.4
12 PM - 3 PM	after	1.1	1	0.856	0.989	0.985	6.619	0.694	-7.12	54.13	2.4
12 PM - 3 PM	after	1.2	1	0.858	0.989	0.985	6.621	0.695	-6.45	54.04	2.4
3 PM - 6 PM	before	-	-	0.755	0.972	0.973	6.504	0.612	0.00	0.00	-
3 PM - 6 PM	after	0.9	1	0.842	0.985	0.983	6.526	0.668	-10.22	54.11	2.4
3 PM - 6 PM	after	1.0	1	0.844	0.986	0.983	6.528	0.670	-10.01	54.65	2.4
3 PM - 6 PM	after	1.1	1	0.848	0.986	0.983	6.531	0.673	-8.47	54.68	2.3
3 PM - 6 PM	after	1.2	1	0.851	0.986	0.983	6.534	0.675	-5.75	54.71	2.4
6 PM - 9 PM	before	-	-	0.761	0.974	0.975	6.561	0.622	0.00	0.00	-
6 PM - 9 PM	after	0.9	1	0.824	0.983	0.981	6.589	0.668	-8.98	49.95	2.5
6 PM - 9 PM	after	1.0	1	0.832	0.985	0.982	6.594	0.673	-6.42	50.35	2.5
6 PM - 9 PM	after	1.1	1	0.834	0.985	0.982	6.597	0.676	-3.56	50.43	2.5
6 PM - 9 PM	after	1.2	1	0.837	0.985	0.982	6.599	0.677	-1.92	50.51	2.5
9 PM - 12 AM	before	-	-	0.755	0.974	0.975	6.487	0.640	0.00	0.00	-
9 PM - 12 AM	after	0.9	1	0.843	0.985	0.982	6.565	0.713	-16.11	54.32	3.5
9 PM - 12 AM	after	1.0	1	0.848	0.985	0.982	6.569	0.716	-15.59	54.41	3.6
9 PM - 12 AM	after	1.1	1	0.849	0.985	0.982	6.572	0.718	-14.72	54.39	3.6
9 PM - 12 AM	after	1.2	1	0.857	0.987	0.984	6.579	0.723	-12.40	54.12	3.6
12 AM - 3 AM	before	-	-	0.773	0.976	0.976	6.586	0.666	0.00	0.00	-
12 AM - 3 AM	after	0.9	1	0.853	0.991	0.988	6.644	0.738	-12.97	50.10	4.1
12 AM - 3 AM	after	1.0	1	0.856	0.991	0.988	6.648	0.741	-12.22	50.23	4.0
12 AM - 3 AM	after	1.1	1	0.862	0.991	0.988	6.654	0.745	-10.23	50.07	4.1
12 AM - 3 AM	after	1.2	1	0.864	0.991	0.988	6.658	0.748	-8.61	49.83	4.1